nature cardiovascular research

Article

https://doi.org/10.1038/s44161-025-00699-x

p22^{phox} prevents the oxidation of SERCA2a and stabilizes it in the heart

Received: 30 July 2024

Accepted: 28 July 2025

Published online: 3 September 2025

Check for updates

Yasuki Nakada[1,2,6], Allen Sam Titus[1,6], Wataru Mizushima[1], Yanfei Yang[1], Peiyong Zhai[1], Yimin Tian[1], Shinichi Oka[1], Toshihide Kashihara[1], Nadezhda Fefelova[1], Sri Harika Pamarthi[1], Tong Liu[3], Hong Li[3], Lai-Hua Xie[1], Koichiro Takayama[1], Soichiro Ikeda[1], Masato Matsushita[1], Chun Yang Huang[4,5], Chiao-Po Hsu[4,5], Kenji Onoue[2], Yoshihiko Saito[2] & Junichi Sadoshima[1]

Sarcoplasmic/endoplasmic reticulum (SR/ER) Ca^{2+} ATPase 2a (SERCA2a) mediates Ca^{2+} reuptake into the SR in cardiomyocytes. The inactivation or downregulation of SERCA2a leads to reduced contractility in the failing heart. Here we show that SERCA2a is regulated by p22^{phox}, a heterodimeric partner of NADPH oxidases. Endogenous p22^{phox} was upregulated by pressure overload, but cardiac-specific p22^{phox} knockout (cKO) in mice exacerbated heart failure, enhanced the downregulation of SERCA2a and increased oxidative stress in the SR. We show that p22^{phox} interacts with SERCA2a, preventing its oxidation at Cys498 and subsequent degradation by the Smurf1 and Hrd1 E3 ubiquitin ligases. The exacerbation of SERCA2a downregulation and cardiac dysfunction following pressure overload in p22^{phox} cKO mice was alleviated when these mice were crossed with SERCA2a-C498S knock-in mice, in which the oxidation-susceptible and degradation-promoting cysteine residue is mutated. Future molecular interventions to prevent the oxidation of SERCA2a at Cys498 may prevent its downregulation during heart failure.

One of the major causes of reduced contractility in the failing heart is impaired Ca^{2+} cycling between the sarcoplasm and the sarcoplasmic reticulum. The increased leakiness of ryanodine receptor 2 (RyR2), potentiated activity of phospholamban (PLN)[1] and downregulation of sarcoplasmic/endoplasmic reticulum (SR/ER) Ca^{2+}-ATPase 2a (SERCA2a)[2] are major drivers of heart failure progression. SERCA2a mediates Ca^{2+} reuptake into the SR/ER Ca^{2+} store from which Ca^{2+} is released through RyR2 for contraction, thereby having fundamental roles in controlling both cardiac relaxation and contraction. Thus, restoration of SERCA2a activity has been an important goal for preventing heart failure progression[3]. Importantly, however, rescue of SERCA2a downregulation by adeno-associated virus 9 (AAV9)-mediated delivery of SERCA2a, although effective in animals, does not appear to be effective in humans. Complex posttranslational modifications of SERCA2a, including oxidation, SUMOylation and acetylation, may prevent effective restoration of SERCA2a function with the current strategy[4].

Elevation of oxidative stress caused by increased electron leakage from damaged mitochondria, elevated production of reactive oxygen species (ROS) from enzymatic sources such as NADPH oxidases and downregulation of antioxidants is a major mechanism driving the progression of heart failure[5]. Under oxidative stress, proteins in the heart undergo posttranslational modification on cysteine residues that can modify functions crucial for cardiomyocyte (CM) survival and homeostasis[6]. We have shown that the function of key signaling

[1]Department of Cell Biology and Molecular Medicine, Cardiovascular Research Institute, Rutgers New Jersey Medical School, Newark, NJ, USA. [2]Department of Cardiovascular Medicine, Nara Medical University, Kashihara, Japan. [3]Center for Advanced Proteomics Research, Department of Microbiology, Biochemistry, and Molecular Genetics, Rutgers New Jersey Medical School and Cancer Institute of New Jersey, Newark, NJ, USA. [4]Division of Cardiovascular Surgery, Department of Surgery, Taipei Veterans General Hospital, Taipei, Taiwan. [5]Institute of Clinical Medicine, School of Medicine, National Yang-Ming University, Taipei, Taiwan. [6]These authors contributed equally: Yasuki Nakada, Allen Sam Titus. e-mail: sadoshju@njms.rutgers.edu

proteins, including HDAC4 (ref. 7), AMPK (ref. 8), mTOR (ref. 9) and Atg7 (ref. 10), in the heart is modulated by oxidation of cysteine residues, which in turn regulates various functions in the heart, including hypertrophy, survival, mitochondrial function and autophagy (reviewed in ref. 6). Cardiac stress disrupts the quality control mechanism of the SR/ER and induces accumulation of mis- and unfolded–damaged proteins, termed ER stress, which is often accompanied by elevated oxidative stress[11]. Together with electron leakage from mitochondria located nearby, elevated oxidative stress, in turn, effectively causes cysteine oxidation of SR/ER proteins, including SERCA2a. Although previous studies have shown that cysteine oxidation affects either the activity or the stability SERCA2a (refs. 12,13), the involvement of cysteine oxidation in SERCA2a downregulation during heart failure and the precise underlying mechanism through which oxidation of SERCA2a cysteine is regulated are poorly understood.

We report that $p22^{phox}$, known as a component of the NADPH oxidase (Nox), regulates cysteine oxidation and degradation of SERCA2a during heart failure. Mice with cardiac-specific deletion of $p22^{phox}$ are more susceptible to heart failure during pressure overload even though the bulk production of ROS is attenuated. Unexpectedly, the knockdown of $p22^{phox}$ leads to increased ER-specific ROS production and oxidation of SERCA2a. On the other hand, $p22^{phox}$ directly binds to SERCA2a, protects it from oxidation of cysteine residues and prevents proteasome-mediated degradation of SERCA2a during oxidative stress. These results suggest that $p22^{phox}$ has a previously unrecognized role in regulating (protecting) the function of SERCA2a through direct interaction. Thus, the goals of this study were to clarify how $p22^{phox}$ affects cysteine oxidation and the function of SERCA2a in the heart and to reveal the molecular mechanism through which cysteine oxidation and the function of SERCA2a are regulated in the heart during heart failure caused by pressure overload.

Results

$p22^{phox}$ is upregulated in the failing human heart and in cardiomyocytes in response to pressure overload

The level of $p22^{phox}$ was evaluated in heart samples obtained from patients with dilated or ischemic cardiomyopathy and from donors with normal hearts. The level of $p22^{phox}$ was significantly higher in the patients' hearts than in the control hearts (Fig. 1a,b and Supplementary Table 1).

To assess the effects of pressure overload, we subjected mice to transverse aortic constriction (TAC) or sham surgery. $p22^{phox}$ expression in the heart was significantly elevated at both mRNA and protein levels after 1 week and 4 weeks of TAC (Fig. 1c–e). $p22^{phox}$ was also upregulated at the mRNA (Fig. 1f) and protein (Fig. 1g,h) levels in cardiomyocytes isolated from wild-type (WT) mice after 1 week of TAC, suggesting that $p22^{phox}$ is produced and upregulated in cardiomyocytes in response to pressure overload.

$p22^{phox}$ cKO mice developed exacerbated heart failure in response to pressure overload

To investigate the role of endogenous $p22^{phox}$ in the heart, we generated cardiomyocyte-specific $p22^{phox}$ knockout ($p22^{phox}$ cKO) mice (Supplementary Fig. 1a,b). As $p22^{phox}$ is also expressed in non-myocytes, residual protein was still detectable in whole hearts (Supplementary Fig. 1c,d). However, the *p22phox* mRNA was significantly reduced in isolated cardiomyocytes from $p22^{phox}$ cKO mice (Supplementary Fig. 1e), and TAC-induced upregulation of $p22^{phox}$ observed in control mice was absent in $p22^{phox}$ cKO cardiomyocytes (Supplementary Fig. 1f), confirming successful gene deletion. At baseline, $p22^{phox}$ cKO mice showed normal cardiac structure and function (Supplementary Tables 2 and 3). However, following 1 week or 4 weeks of TAC, $p22^{phox}$ cKO mice developed more severe left ventricle (LV) dilation (increased LV end-diastolic diameter (LVEDD) and LV end-systolic diameter (LVESD)) and greater LV dysfunction (reduced LV ejection fraction (LVEF)) than control mice (Fig. 2a–e). In addition, lung congestion and LV end-diastolic pressure (LVEDP) were significantly increased after 4 weeks of TAC in $p22^{phox}$ cKO mice (Fig. 2f,g), and aortic pressure gradients were reduced (Fig. 2h), consistent with impaired contractility. These mice also showed a blunted inotropic response to dobutamine (Supplementary Fig. 2a–d), indicating reduced cardiac reserve. Histological analyses show that the cardiomyocyte cross-sectional area (CSA) was comparable between groups after TAC (Fig. 2i,j), but fibrosis was significantly exacerbated in $p22^{phox}$ cKO hearts (Fig. 2k,l). Importantly, survival after TAC was markedly lower in $p22^{phox}$ cKO mice (Fig. 2m). Collectively, these findings show that although $p22^{phox}$ is dispensable at baseline, its absence impairs the heart's ability to compensate under pressure overload, leading to worsened LV dysfunction, enhanced fibrosis and increased mortality.

LC–MS/MS identified binding of $p22^{phox}$ and SERCA2a

To uncover how $p22^{phox}$ loss contributes to cardiac dysfunction under pressure overload, we searched for $p22^{phox}$-binding proteins. Lysates from adult mouse cardiomyocytes were incubated with or without Flag-tagged $p22^{phox}$, followed by anti-Flag immunoprecipitation. Interacting proteins were identified using liquid chromatography with tandem mass spectrometry (LC–MS/MS) with spectral counting. We identified 555 proteins by LC–MS/MS, of which 231 proteins bound well to Flag–$p22^{phox}$ (ratio > 1.5) with respect to the control group (Supplementary Table 4). The LC–MS/MS analysis showed that SERCA2a was the protein that bound most abundantly to Flag–$p22^{phox}$ in the mouse heart.

$p22^{phox}$ binds directly to SERCA2a

To further validate the interaction between $p22^{phox}$ and SERCA2a, co-immunoprecipitation revealed that SERCA2a was specifically detected in anti-$p22^{phox}$ immunoprecipitates, but not when a non-specific control antibody was used (Fig. 3a). Conversely, $p22^{phox}$ was detected in the immunoprecipitate with anti-SERCA2a antibody (Fig. 3b). These results suggest that $p22^{phox}$ and SERCA2a physically interact with one another. A direct interaction between SERCA2a and $p22^{phox}$ was confirmed by in vitro binding assays using recombinant proteins (Fig. 3c). This interaction was further validated in cells using a proximity ligation assay (PLA), which revealed robust signals in the perinuclear region of cardiomyocytes when both anti-$p22^{phox}$ and anti-SERCA2a antibodies were applied, consistent with the complex formation in the sarcoplasmic reticulum (Fig. 3d). To map the interaction domain, a series of SERCA2a deletion mutants were tested. $p22^{phox}$ bound to full-length SERCA2a, as well as SERCA2a 1–666, 334–666 and 334–998 constructs, but not to SERCA2a 1–333, identifying the 334–666 amino acid region as necessary for binding (Fig. 3e).

$p22^{phox}$ cKO mice showed abnormal Ca^{2+} handling

As SERCA2a transports cytosolic Ca^{2+} into the SR, Ca^{2+} transients were measured in isolated cardiomyocytes. At baseline, $p22^{phox}$ cKO cardiomyocytes showed a significantly reduced peak amplitude compared with the control (Fig. 4a,b). The peak amplitude of the Ca^{2+} transient after caffeine administration, indicating the total SR Ca^{2+} content, was then evaluated. At baseline, a rapid caffeine spike emptying the intracellular Ca^{2+} store in single cardiomyocytes revealed a significantly reduced SR Ca^{2+} content in the $p22^{phox}$ cKO mouse cardiomyocytes compared with in the control mouse cardiomyocytes (Fig. 4c). There was no significant difference in the percentage of fractional Ca^{2+} release between control and $p22^{phox}$ cKO cardiomyocytes at baseline (Fig. 4d). The decay constant of the Ca^{2+} transient (tau) was significantly greater in cardiomyocytes isolated from $p22^{phox}$ cKO mice than in those from control mice at baseline (Fig. 4e). The Ca^{2+} transients were also assessed in isolated cardiomyocytes after 1 week of pressure overload (TAC). The peak amplitude and the total SR Ca^{2+} content were significantly lower in the $p22^{phox}$ cKO mouse cardiomyocytes than in the control mouse cardiomyocytes after 1 week of TAC (Fig. 4a–c). There was no significant difference in the percentage of fractional Ca^{2+} release between control

https://doi.org/10.1038/s44161-025-00699-x

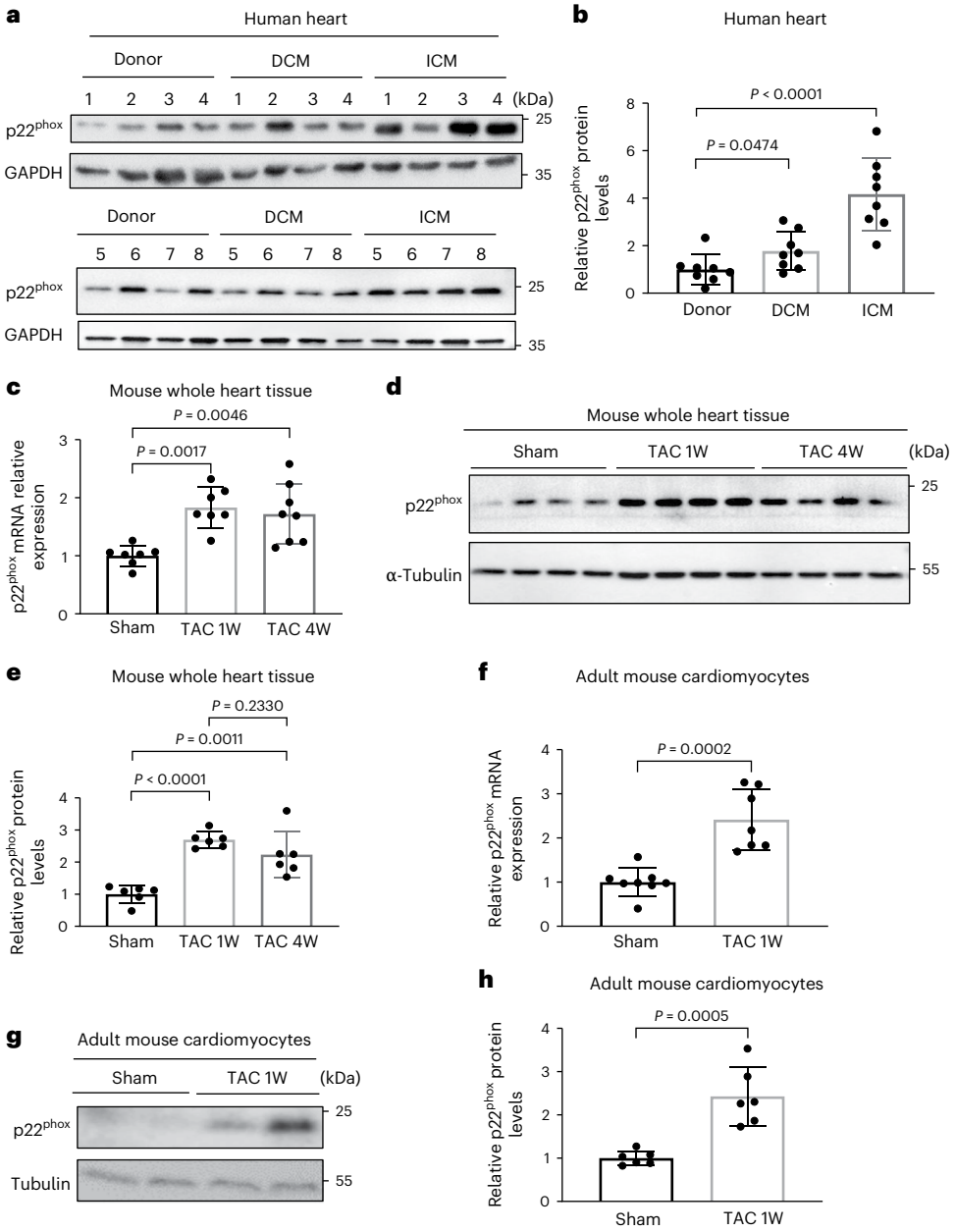

Fig. 1 | p22^{phox} is upregulated in the failing human heart and in cardiomyocytes in response to pressure overload. a,**b**, Human heart LV samples obtained from healthy donor hearts and from patients with DCM or ICM were analyzed for p22^{phox} protein expression levels ($n = 8$). **a**, The protein levels of p22^{phox}, analyzed by western blotting with GAPDH as a loading control, in normal, DCM and ICM human heart LV lysates. **b**, Relative p22^{phox} protein levels. **c**–**e**, Mice were subjected to TAC (1 week (1W) or 4 weeks (4W)) or sham operation, and the pressure gradient was assessed by Doppler on day 2 to confirm that appropriate levels of constriction were applied. After TAC, the heart LV tissues were analyzed for mRNA and protein expression. **c**, Relative *p22^{phox}* mRNA levels (Sham and TAC 1W $n = 7$ and TAC 4W $n = 8$). **d**, The protein levels of p22^{phox} were analyzed from whole heart tissue by western blotting with tubulin as loading control. **e**, The relative p22^{phox} protein levels ($n = 6$). **f**–**h**, Following TAC 1W or sham operation, cardiomyocytes were isolated from adult mouse heart LV tissue and analyzed for protein and mRNA expression. **f**, The *p22^{phox}* mRNA levels (Sham $n = 8$ and TAC 1W $n = 7$). **g**, The protein levels of p22^{phox}, analyzed by western blotting with tubulin as loading control. **h**, The relative p22^{phox} protein levels ($n = 6$). All bar graphs represent the mean ± s.e. Statistical significance was determined using one-way ANOVA with Tukey test (**b**, **c** and **e**) and unpaired Student's *t*-test (two tailed) (**e**, **f** and **h**).

and p22^{phox} cKO cardiomyocytes after 1 week of TAC (Fig. 4d). The tau was significantly greater in cardiomyocytes isolated from p22^{phox} cKO mice than in those from control mice after TAC (Fig. 4e). These results are consistent with the notion that the activity of SERCA2a is reduced in p22^{phox} cKO cardiomyocytes both at baseline and after TAC. On the other hand, the tau for the decay of Ca^{2+} transient after caffeine administration, reflecting the activity of the Na^{+}/Ca^{2+} exchanger (NCX)[14], was not significant between control and p22^{phox} cKO mice at baseline and after TAC (Fig. 4f), although it was significantly smaller after TAC compared with the sham operation in p22^{phox} cKO mice, suggesting compensatory activation of NCX.

p22^{phox} posttranscriptionally regulates SERCA2a protein levels

Given altered calcium handling in p22^{phox} cKO mice, we examined how endogenous p22^{phox} regulates key cardiac calcium handling genes at baseline and 1 week after pressure overload. The relative mRNA levels of SERCA2a, PLN, NCX and ryanodine receptor (RyR) were not significantly different between control and p22^{phox} cKO mice at baseline (Fig. 5a,b

https://doi.org/10.1038/s44161-025-00699-x

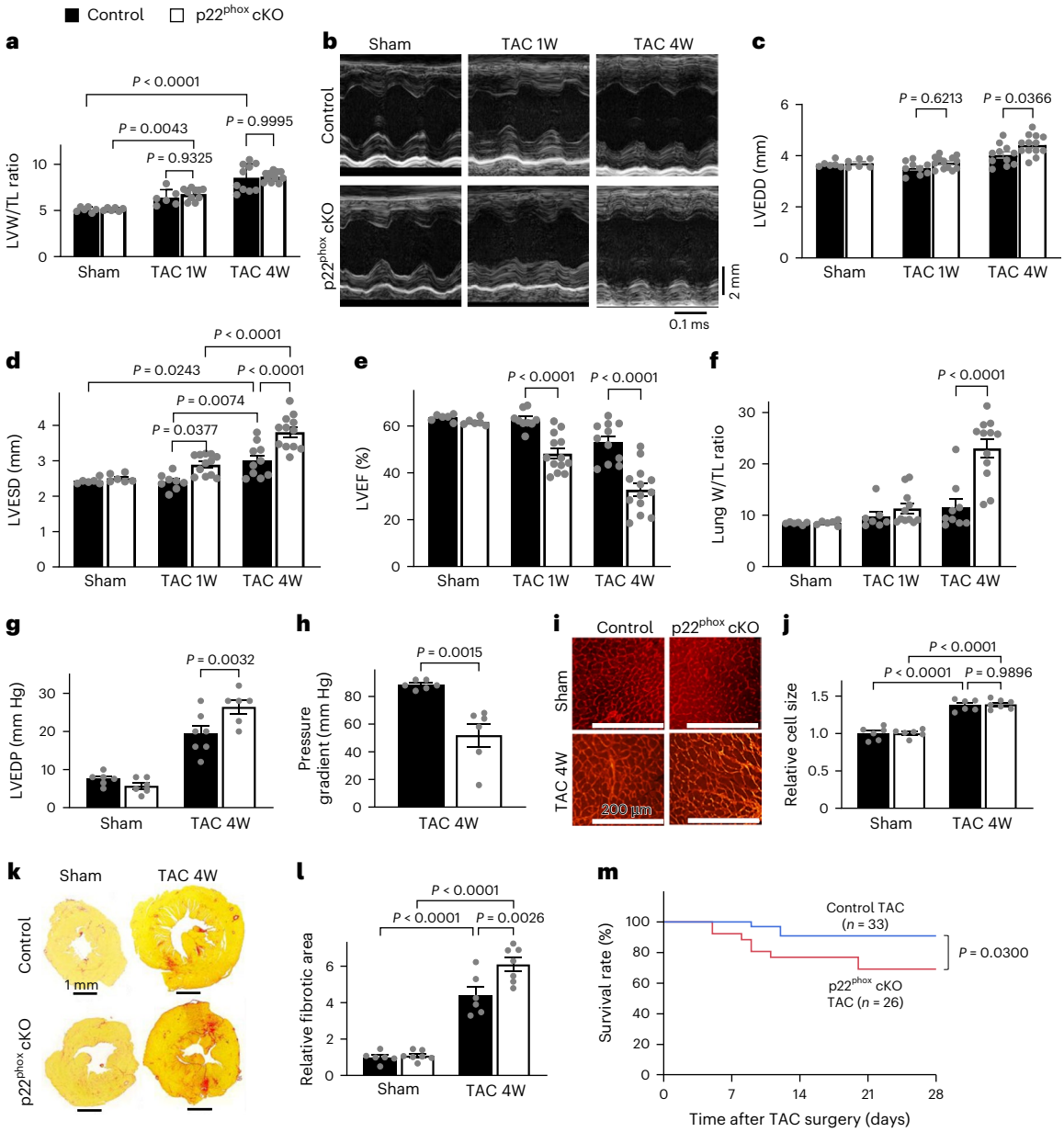

Fig. 2 | p22^{phox} cKO mice developed exacerbated heart failure in response to pressure overload. a–**h**, Control mice and p22^{phox} cKO (homozygous) mice were subjected to sham operation or TAC (1W or 4W), and the pressure gradient was assessed by Doppler on day 2 to confirm that appropriate levels of constriction were applied. The mice were then analyzed for hypertrophic response and cardiac function by echocardiography. **a**, The hearts were collected, and the LVW (in mg) was measured and divided by the TL (in mm). The relative LV weight to tibia length (LVW/TL) ratio was plotted to compare the hypertrophic response (control: sham $n = 6$, TAC 1W $n = 6$, TAC 4W $n = 10$; p22^{phox} cKO: sham $n = 6$, TAC 1W $n = 10$, TAC 4W $n = 12$). **b**, Representative echocardiographs from control and p22^{phox} cKO mice subjected to sham operation or TAC (1W or 4W). **c**, LVEDD analyzed by echocardiography (control: sham $n = 6$, TAC 1W $n = 9$, TAC 4W $n = 11$; p22^{phox} cKO: sham $n = 6$, TAC 1W $n = 13$, TAC 4W $n = 13$). **d**, LVESD analyzed by echocardiography (control: sham $n = 6$, TAC 1W $n = 8$, TAC 4W $n = 10$; p22^{phox} cKO: sham $n = 6$, TAC 1W $n = 12$, TAC 4W $n = 12$). **e**, LVEF analyzed by echocardiography (control: sham $n = 6$, TAC 1W $n = 9$, TAC 4W $n = 11$; p22^{phox} cKO: sham $n = 6$, TAC 1W $n = 13$, TAC 4W $n = 13$). **f**, The LungW (in mg) was measured and divided by the TL (in mm). The relative lung W/TL ratio was plotted to compare the extent of lung congestion (control: sham $n = 6$, TAC 1W $n = 7$, TAC 4W $n = 9$; p22^{phox} cKO: sham $n = 6$, TAC 1W $n = 11$, TAC 4W $n = 12$). **g**,**h**, Hemodynamic measurements were obtained by catheterization from control and p22^{phox} cKO (homozygous) mice that were subjected to sham operation or TAC (4W). **g**, LVEDP (control: sham $n = 6$, TAC 4W $n = 7$; p22^{phox} cKO: sham $n = 6$, TAC 4W $n = 6$). **h**, Pressure gradient ($n = 6$). **i**–**l**, Histological evaluation of hypertrophy and fibrosis in control mice and p22^{phox} cKO (homozygous) mice subjected to sham operation or TAC (4W). **i**, Wheat germ agglutinin staining showing cell size. **j**, Relative cell size (control: sham $n = 6$, TAC 4W $n = 7$; p22^{phox} cKO: sham $n = 6$, TAC 4W $n = 6$). **k**, Picrosirius red staining. **l**, Relative fibrotic area fold change (control: sham $n = 6$, TAC 4W $n = 6$; p22^{phox} cKO: sham $n = 7$, TAC 4W $n = 7$). **m**, Percentage survival in days after TAC surgery by Kaplan–Meier analysis with log rank test. All bar graphs represent the mean ± s.e. Statistical significance was determined using one-way ANOVA with Tukey test (**a**, **c**, **d** and **j**), one-way ANOVA with Šidák's multiple-comparison test (**e**–**g** and **l**) and unpaired Student's *t*-test (two tailed) (**h**).

and Supplementary Fig. 2e,f). Although the levels of *SERCA2a*, *PLN* and *RyR* mRNA expression were significantly decreased in both p22^{phox} cKO and control mice after 1 week of pressure overload, there was no significant difference between p22^{phox} cKO and control mice (Fig. 5a and Supplementary Fig. 2f). As p22^{phox} interacts with SERCA2a, we examined SERCA2a protein levels. Despite there being no change in the mRNA, the SERCA2a protein was significantly reduced in p22^{phox} cKO mice compared with controls, both at baseline and after pressure

https://doi.org/10.1038/s44161-025-00699-x

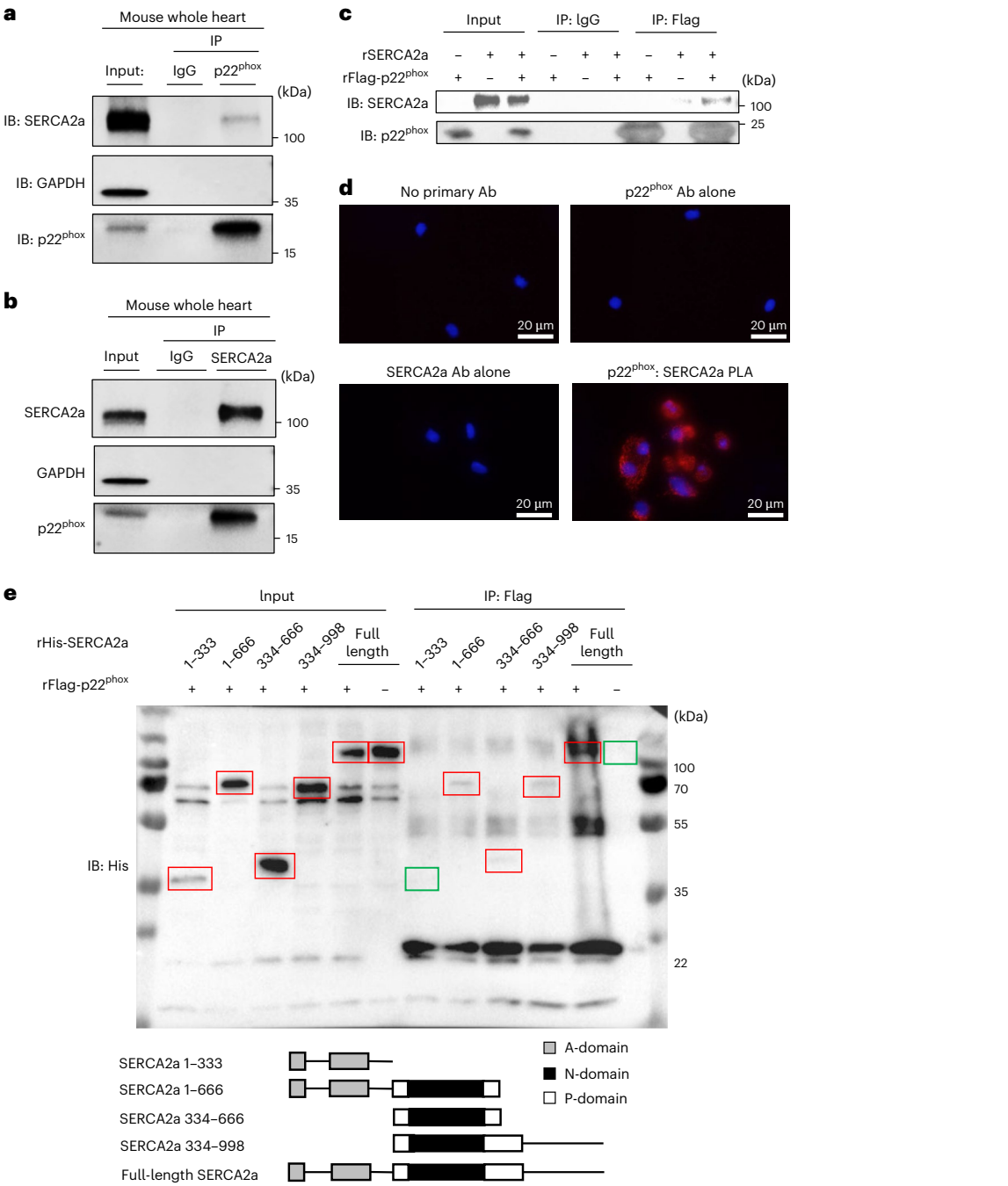

Fig. 3 | p22^{phox} binds directly to SERCA2a. a,**b**, Immunoprecipitation (IP) of p22^{phox} and SERCA2a from mouse whole heart tissue lysates using specific antibodies and with respective IgG control. Immunoprecipitates were loaded along with a 10% input fraction and immunoblotted (IB) for SERCA2a and p22^{phox} protein. **a**, Immunoprecipitation of p22^{phox} with co-immunoprecipitation of SERCA2a (performed at least three times independently). **b**, Immunoprecipitation of SERCA2a with co-immunoprecipitation of p22^{phox} (performed at least three times independently). **c**, In vitro binding assay. Recombinant SERCA2a (rSERCA2a) and recombinant Flag-tagged p22^{phox} (rFlag-p22^{phox}) were incubated in IP cell lysis buffer and immunoprecipitated. The Flag-tagged p22^{phox}, along with IgG control and the immunoprecipitated complexes, was washed and immunoblotted for SERCA2a and p22^{phox}. The blots show binding of recombinant Flag-tagged p22^{phox} (rFlag-p22^{phox}) with rSERCA2a (performed at least three times independently). **d**, PLA performed in neonatal rat cardiomyocytes. Cardiomyocytes were incubated with antibody diluent alone, rabbit anti-p22^{phox} antibody alone, mouse anti-SERCA2a alone, and anti-p22^{phox} and anti-SERCA2a antibodies for 2 h at 37 °C. Five random images per well were acquired using DAPI (blue nuclei) and Cy5 filters (red Cy5 PLA fluorescence signals are a result of the secondary antibody-conjugated PLA probe ligation and amplification only in the presence of antibodies against both p22^{phox} and SERCA2a, indicating close proximity (<40 nm)) (performed at least three times independently). **e**, Top: in vitro binding of different fragments of recombinant His-tagged SERCA2a (rHis-SERCA2a) with Flag-tagged p22^{phox} (rFlag-p22^{phox}). SERCA2a His-tagged serial truncations were individually incubated with rFlag-p22^{phox}, then pulled down with anti-Flag M2 beads and immunoblotted with anti-His antibody. The red rectangles indicate the different lengths of recombinant His-tagged SERCA2a (rHis-SERCA2a), seen in the input fraction and the immunoprecipitated lanes that bound to recombinant Flag-tagged p22^{phox} (rFlag-p22^{phox}) (performed at least three times independently). The green rectangles indicate absence of immunoprecipitated bands. Bottom: a schematic representation of the SERCA2a domain structure (three cytoplasmic domains (boxes): the actuator domain (A-domain), the nucleotide binding domain (N-domain) and the phosphorylation domain (P-domain), and transmembrane domains (lines)).

https://doi.org/10.1038/s44161-025-00699-x

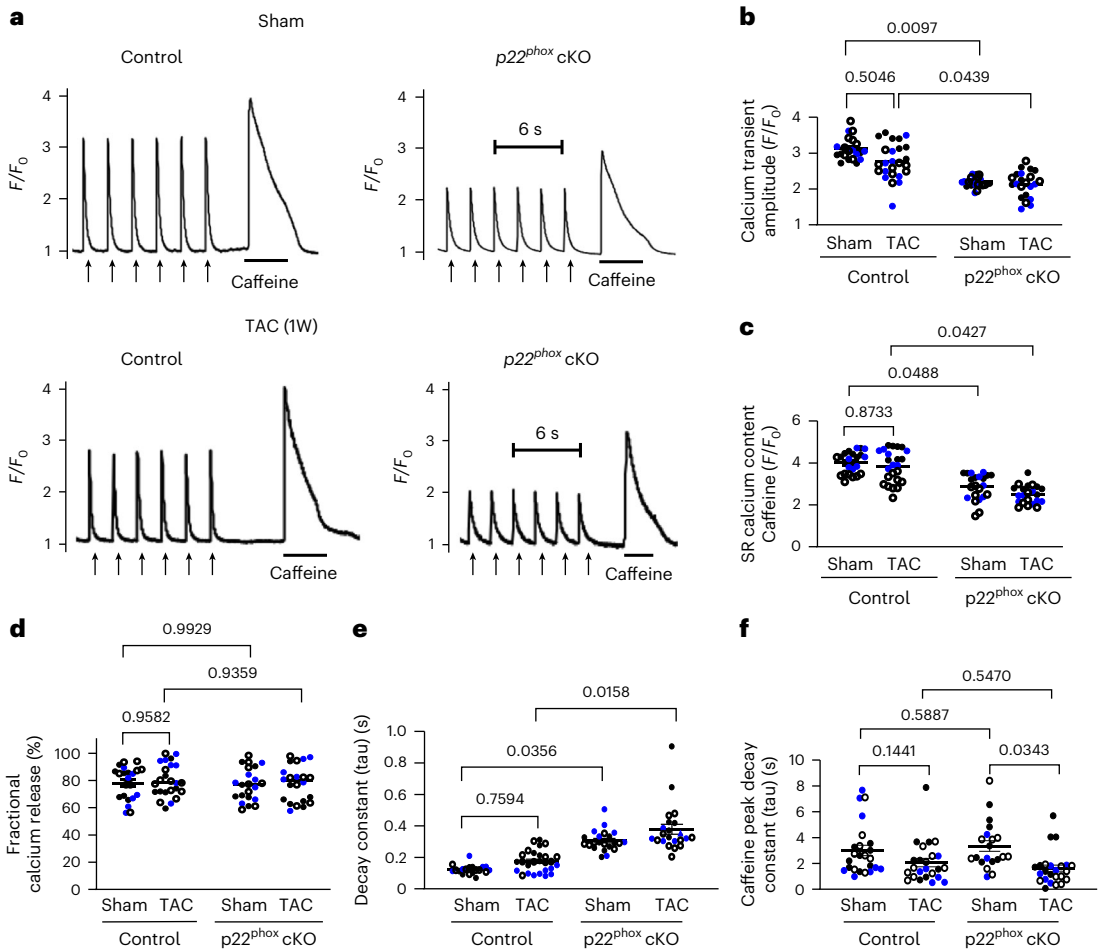

Fig. 4 | p22^{phox} cKO mice showed abnormal Ca^{2+} handling. a–f, Ca^{2+} transient and SR Ca^{2+} content in p22^{phox} cKO myocytes at baseline and after 1-week TAC. Adult cardiomyocytes were isolated from control and p22^{phox} cKO mice using the Langendorff perfusion method. The cardiomyocytes were loaded with Fluo-4 AM. Ca^{2+} fluorescence intensity was recorded as the ratio of the fluorescence (F) over the basal diastolic fluorescence (F_0). **a**, Twitch Ca^{2+} transient and SR Ca^{2+} content measured as the height of the caffeine (10 mM)-induced Ca^{2+} transient in representative ventricular myocytes from control and p22^{phox} cKO mice at baseline and 1 week after TAC. Ca^{2+} fluorescence intensity was recorded as the ratio F/F_0 of the fluorescence (F) over the basal diastolic fluorescence (F_0). **b–f**, Summarized data for twitch representing the mean ± s.e. from three mice per condition and specified number of cells per mouse Ca^{2+} transient amplitude (WT: sham−6, 6, 9, TAC−7, 9, 9; p22^{phox} cKO: sham−8, 8, 8, TAC−8, 7, 7) (**b**), SR Ca^{2+} content (WT: sham−7, 7, 8, TAC−7, 7, 10; p22^{phox} cKO: sham−7, 7, 8, TAC−7, 7, 8) (**c**), fractional SR Ca^{2+} release (WT: sham−7, 7, 8, TAC−7, 7, 10; p22^{phox} cKO: sham−7, 7, 8, TAC−7, 7, 8) (**d**), decay constant (tau) (WT: sham−6, 6, 7, TAC−7, 9, 11; p22^{phox} cKO: sham−8, 7, 7, TAC−6, 6, 10) (**e**) and caffeine peak decay constant (tau) (WT: sham−8, 8, 8, TAC−8, 6, 10; p22^{phox} cKO: sham−8, 3, 9, TAC−8, 6, 10) (**f**) in control and p22^{phox} cKO ventricular myocytes at baseline and after 1-week TAC. The individual data points from cells of each mouse are represented by dots (filled black and blue dots and black empty dots). The statistical analysis was conducted using the nested *t*-test (two tailed) (**c** and **f**), nested one-way ANOVA and Tukey's multiple-comparison test (**b** and **e**), and nested one-way ANOVA and Šidák's multiple-comparison test (**d**). Hierarchical clustering dendrogram analysis was performed, and the dendrogram is provided in the source data.

overload (Fig. 5c,d). Similarly, in cultured neonatal rat cardiomyocytes with small interfering RNA-mediated p22^{phox} knockdown, *SERCA2a* mRNA levels were unaltered but the protein level of SERCA2a was significantly smaller after p22^{phox} knockdown (Fig. 5e–g). These results suggest that p22^{phox} may control the SERCA2a protein level through posttranscriptional mechanisms. PLN inhibits SERCA2a, but this inhibition is relieved upon phosphorylation by protein kinase A (ref. 15). In p22^{phox} cKO mice, phosphorylated phospholamban protein levels were significantly higher than in controls, suggesting a compensatory response to reduced SERCA2a (Fig. 5h,i). Relative ATPase activity in isolated SR fractions from control and p22^{phox} cKO mice showed no significant difference when normalized to SERCA2a levels (Fig. 5j).

SERCA2a overexpression attenuated pressure overload-induced LV dysfunction in p22^{phox} cKO mice

To show the role of SERCA2a downregulation in cardiac dysfunction in p22^{phox} cKO mice under pressure overload, we performed rescue experiments using cardiomyocyte-specific SERCA2a expression via AAV9–cTnT–SERCA2a. Injection of AAV9–cTnT–SERCA2a increased cardiac SERCA2a expression in both control and p22^{phox} cKO mice in both the sham and TAC groups (Extended Data Fig. 1a–d). No significant difference in LV tissue weight (LVW)/tibia length (TL) was observed in the presence of SERCA2a overexpression either after the sham operation or 4 weeks after TAC compared with in an eGFP overexpression group (control) (Extended Data Fig. 1e). The increase in lung weight observed after 4 weeks of TAC in p22^{phox} cKO mice was attenuated in p22^{phox} cKO mice injected with AAV9–cTnT–SERCA2a (Extended Data Fig. 1f). Moreover, LVEF after 4 weeks of TAC was significantly reduced in p22^{phox} cKO mice, but not in p22^{phox} cKO mice injected with AAV9–cTnT–SERCA2a (Extended Data Fig. 1g). These data suggest that supplementation of SERCA2a levels in cardiomyocytes rescues cardiac dysfunction associated with a lack of p22^{phox}. Thus, SERCA2a downregulation has an important role in mediating cardiac dysfunction in p22^{phox} cKO mice.

https://doi.org/10.1038/s44161-025-00699-x

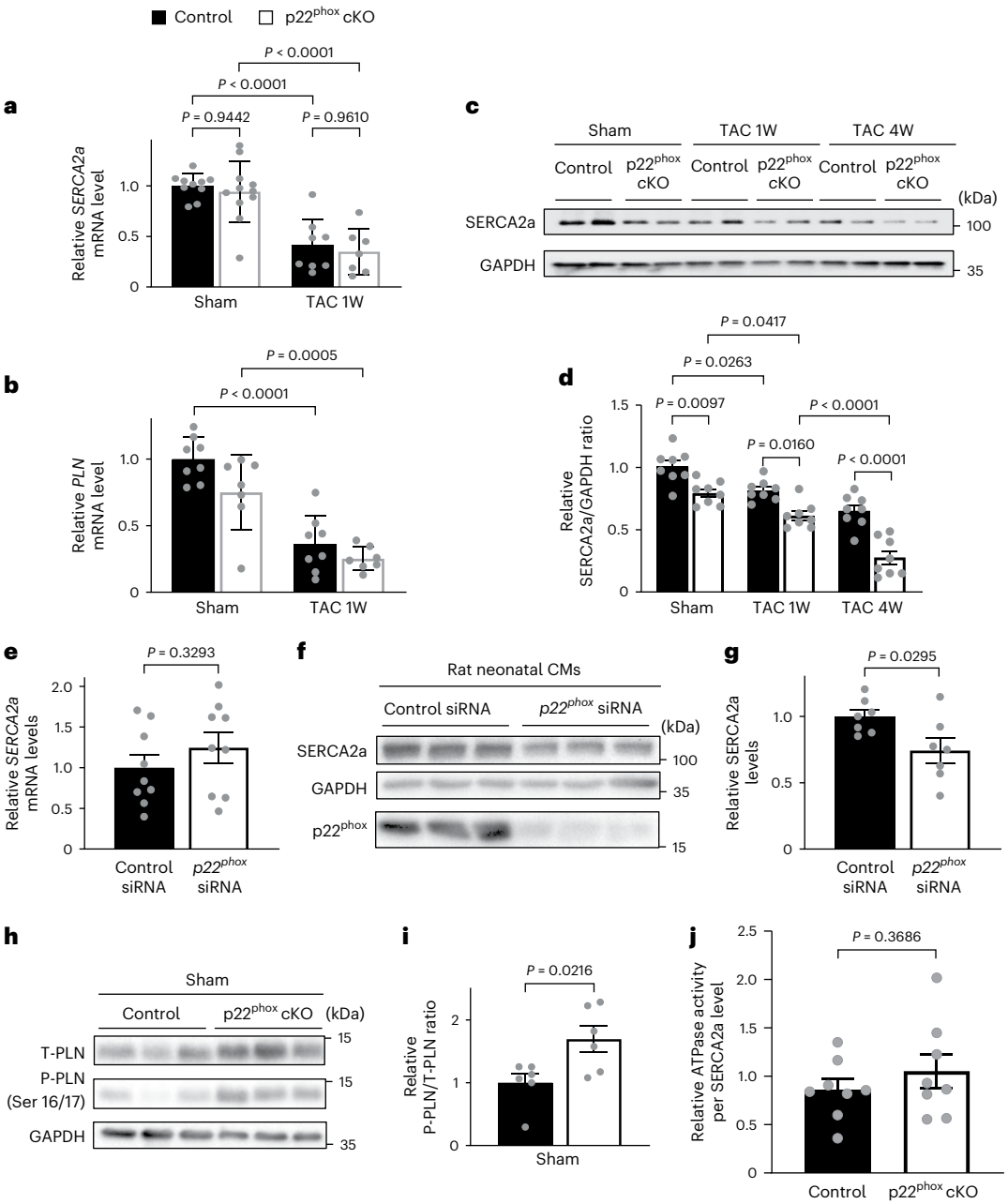

Fig. 5 | p22^{phox} posttranscriptionally regulates SERCA2a protein levels. **a**–**d**, Mouse heart tissues from control and p22^{phox} cKO mice after sham operation or 1-week TAC were analyzed for mRNA by quantitative PCR and protein expression by immunoblotting. **a**, Relative *SERCA2a* mRNA expression in the hearts of control and p22^{phox} cKO mice (sham: WT−10, p22^{phox} cKO−11; TAC 1W: WT−8, p22^{phox} cKO−7). **b**, Relative *PLN* mRNA expression in the hearts of control and p22^{phox} cKO mice (sham: WT−10, p22^{phox} cKO−11; TAC 1W: WT−8, p22^{phox} cKO−7). **c**, Representative immunoblots from the heart LV tissue lysates of control and p22^{phox} cKO mice after sham and 1-week and 4-week TAC surgery showing changes in SERCA2a protein levels. **d**, Relative SERCA2a protein expression expressed as the ratio of SERCA2a to GAPDH (sham: WT−8, p22^{phox} cKO−8; TAC 1W: WT−8, p22^{phox} cKO−8; TAC 4W: WT−8, p22^{phox} cKO−8). **e**, Relative *SERCA2a* mRNA expression analyzed by quantitative PCR in rat neonatal cardiomyocytes that were transfected with control siRNA or *p22^{phox}* siRNA ($n = 9$). **f**, Representative immunoblots of SERCA2a from rat neonatal cardiomyocyte lysates that were transfected with control siRNA or *p22^{phox}* siRNA. **g**, Relative SERCA2a protein levels after normalization to GAPDH ($n = 7$). **h**, Representative immunoblots of T-PLN and phosphorylated (serine 16/17)-PLN (P-PLN (Ser 16/17) from the heart LV tissue lysates of control and p22^{phox} cKO mice under the sham condition. **i**, Relative phosphorylated to total phospholamban levels in the heart tissue lysates of control and p22^{phox} cKO mice under the sham condition ($n = 6$). **j**, The SR fraction was isolated from control and p22^{phox} cKO (homozygous knockout) mouse hearts, and the specific SERCA2a ATPase activity of the fraction was assessed and normalized to the SERCa2a level in the SR fraction. The graph shows relative ATPase activity (normalized to SERCA2a levels) in the control and p22^{phox} cKO SR fraction ($n = 8$). All bar graphs represent the mean ± s.e. Statistical significance was determined using one-way ANOVA with Tukey test (**a**, **b** and **d**) and unpaired Student's *t*-test (two tailed) (**e**, **g**, **i** and **j**).

p22^{phox} protected SERCA2a against oxidation and degradation

We investigated how p22^{phox} regulates SERCA2a protein expression, given that SERCA2a is sensitive to oxidative modification, which can promote its degradation or reduce its activity in a context-dependent manner[16]. As p22^{phox} interacts with SERCA2a, and its loss reduces SERCA2a protein levels, we hypothesized that p22^{phox} modulates SERCA2a oxidation.

To assess oxidative stress, we measured total dityrosinated proteins and tissue-released H_2O_2 in p22^{phox} cKO mice. While both markers increased after pressure overload in control and p22^{phox} cKO mouse

hearts, their levels were significantly lower in p22^{phox} cKO mice (Fig. 6a–c). However, ER-localized HyPer fluorescence revealed higher H_2O_2 signals in p22^{phox} knockdown cardiomyocytes compared with controls (Fig. 6d,e and Extended Data Fig. 2a,b), indicating that p22^{phox} loss increases local oxidative stress in the ER, despite lower total cardiac oxidative stress.

As multiple cysteine residues are subjected to oxidative modifications[17,18], the extent of cysteine oxidation in SERCA2a was evaluated by blocking free reactive cysteine thiols with biotinylated iodoacetamide (BIAM) labeling and pull-down. There was significantly less BIAM-labeled SERCA2a in the heart in p22^{phox} cKO mice than in control mice (Fig. 6f,g), indicating that the SERCA2a cysteine residues are more oxidized in p22^{phox} cKO mice than in control mice.

We then evaluated redox-sensitive cysteines in p22^{phox} cKO and control mouse hearts. Reduced free cysteines in the heart at the time of collection were irreversibly labeled with BIAM, whereas oxidized cysteines were first reduced with dithiothreitol (DTT) and then labeled with biotin-free IAM. LC–MS/MS showed that BIAM labeling of 7 cysteines (Cys344/349, Cys447, Cys471, Cys498, Cys560 and Cys669) was reduced by 30% or more in p22^{phox} cKO mouse hearts compared with in control hearts, excluding low-label-efficiency (<1%) cysteines. Although several cysteines in SERCA2a were more oxidized in p22^{phox} cKO mice than in control mice, Cys498 was oxidized to the greatest extent (Fig. 6h). To evaluate the functional significance of Cys498 oxidation, we generated adenoviruses harboring SERCA2a-C498S (Ad–Flag–SERCA2a-C498S) and studied how the Cys498 oxidation resistant mutation affects the overall oxidation status of SERCA2a. Cardiomyocytes transduced with Ad–Flag–SERCA2a-C498S showed significantly less BIAM labeling of Flag–SERCA2a than those transduced with Ad–Flag–SERCA2a WT (Fig. 6i,j). Furthermore, cardiomyocytes transduced with Ad–Flag–SERCA2a-C498S showed no further reduction in the amount of BIAM-labeled Flag–SERCA2a in the absence of p22^{phox} compared with in the presence of p22^{phox}. These results indicate that Cys498 is a major site of cysteine oxidation in SERCA2a in the absence of p22^{phox}. In addition, the decrease in the SERCA2a level in the absence of p22^{phox} was significantly alleviated in the presence of SERCA2a-C498S in cardiomyocytes (Fig. 6k–m). These results suggest that the absence of p22^{phox} results in the oxidation of SERCA2a at Cys498 and negatively affects the protein level of SERCA2a.

To identify the source of H_2O_2 in the ER in the absence of p22^{phox}, we evaluated whether the increased ER-localized oxidative stress is mediated by Nox4, a partner of p22^{phox} in the ER. We have shown previously that a lack of anti-apoptotic HS-1-associated protein X-1 (HAX-1), a regulator of ER-mediated cell survival, leads to increased oxidative stress in the ER through a Nox4-dependent mechanism[12]. The ER-localized HyPer fluorescence ratio was not affected by Nox4 downregulation in either the presence or absence of p22^{phox} knockdown (Extended Data Fig. 2a,b). Although the knockdown of p22^{phox} decreased the protein levels of both Nox4 and SERCA2a, the knockdown of Nox4 did not decrease SERCA2a levels (Extended Data Fig. 2c–e). p22^{phox} downregulation also decreased Nox2 protein levels (Extended Data Fig. 3a,b). These data suggest that upregulation of H_2O_2 and downregulation of SERCA2a in response to p22^{phox} downregulation are independent of Nox4 or Nox2. Furthermore, knockdown of p22^{phox} did not alter the mitochondria-localized Mito-HyPer fluorescence ratio compared with the control (Extended Data Fig. 3e,f), excluding mitochondria-derived oxidative stress in the p22^{phox}-deficient condition. Interestingly, the ER-localized HyPer fluorescence ratio was high when SERCA2a was downregulated (Extended Data Fig. 3e,f). Thus, increased oxidative stress in the ER in response to downregulation of p22^{phox} is associated with SERCA2a downregulation.

SERCA2a undergoes ubiquitination and proteasomal degradation in the absence of p22^{phox}

As the protein level of SERCA2a was downregulated in the absence of p22^{phox}, the possibility of SERCA2a ubiquitination and degradation by the proteasome was investigated. Flag-tagged WT SERCA2a was immunoprecipitated from neonatal rat cardiomyocytes transduced with adenoviruses harboring LacZ or *p22^{phox}* short hairpin RNA and administered epoxomicin, an irreversible selective proteasome inhibitor. SERCA2a was more highly ubiquitinated (K48-linked ubiquitination) in the presence of p22^{phox} downregulation (Supplementary Fig. 3a). Cycloheximide chase assays were conducted in neonatal rat cardiomyocytes expressing either Flag-tagged wild-type SERCA2a or C498S SERCA2a in the presence of either LacZ or *p22^{phox}* shRNA and epoxomicin. Although WT SERCA2a was susceptible to proteasomal degradation in the absence of p22^{phox}, C498S SERCA2a was more stable than WT SERCA2a even in the absence of p22^{phox} (Extended Data Fig. 4a–d). Moreover, siRNA-mediated knockdown of proteasome subunit alpha type-3 (PSMA3), a subunit of the 20S proteasome core and a part of the 26S proteasome, rescued the SERCA2a levels downregulated in the presence of p22^{phox} knockdown (Extended Data Fig. 4e,f), suggesting that SERCA2a undergoes proteasomal degradation in the absence of p22^{phox}.

Fig. 6 | p22^{phox} protected SERCA2a against oxidation and degradation. **a**, Mouse heart tissues from control and p22^{phox} cKO mice after the sham operation or 4-week TAC were analyzed for dityrosine levels (a marker of oxidative stress on tyrosine residues of proteins) by immunoblotting. The figure shows a representative immunoblot for dityrosine levels with GAPDH as loading control. **b**, Quantification of dityrosine protein levels as the ratio of relative dityrosine to GAPDH ($n = 6$). **c**, Mouse heart tissues from control and p22^{phox} cKO mice after the sham operation or 1-week TAC were analyzed for levels of H_2O_2 released using Amplex red reagent by comparison against known H_2O_2 standards. The graph shows H_2O_2 levels in the tissue normalized to the weight of the tissue in mg ($n = 6$). **d**, Rat neonatal cardiomyocytes were transduced with adenoviruses expressing ER-HyPer (ER-targeting ratiometric fluorescence sensor protein that detects H_2O_2 levels) and co-transfected with control siRNA or *p22^{phox}* siRNA. The images shown are representative of the fluorescence ratiometric (excitation peak at 500 nm to excitation peak at 420 nm) images from cells with control siRNA or *p22^{phox}* siRNA (the color scale indicates low to high ROS levels) (performed at least three times independently). **e**, Quantification of the number of high ratio cells to total cells per field from control siRNA or *p22^{phox}* siRNA-treated cells, expressed as a percentage ($n = 5$). **f**, Left ventricular homogenates from control and p22^{phox} cKO mice were incubated with BIAM and pulled down with avidin resin. The pull-down fractions and whole cell lysates (WCL) were immunoblotted for SERCA2a. The figure shows a representative immunoblot of SERCA2a labeled with BIAM from control and p22^{phox} cKO mouse LV lysates. **g**, Quantification of BIAM–SERCA2a normalized by total SERCA2a in control and p22^{phox} cKO mouse LV lysates (data from six mice per group). **h**, The overlay extract ion chromatograms of peptide $SM_{ox}SVYC_{498\text{-}biotin}TPNKPSR$ in control and KO. The PEO-iodoacetyl-LC-biotin modification on cysteine represents the reduced form of cysteine. The dramatic decrease in the amount of the reduced form of cysteine at C498 in the KO indicates that the KO has more oxidized C498. **i**–**m**, Neonatal rat ventricular myocytes (NRVMs) were transduced with Ad–Flag–SERCA2a WT or Ad–Flag–SERCA2a-C498S mutant in the presence or absence of *p22^{phox}* siRNA. **i**, Representative immunoblots of BIAM-labeled Flag-SERCA2a obtained from NRVMs that were transfected with Ad–Flag–SERCA2a WT or Ad–Flag–SERCA2a-C498S mutant in the presence or absence of *p22^{phox}* siRNA. SE, short exposure; LE, long exposure. **j**, Quantification analyses of BIAM–Flag–SERCA2a normalized by total Flag–SERCA2a in **I** ($n = 6$). **k**, Representative immunoblots of Flag–SERCA2a in rat neonatal cardiomyocytes transfected with Ad–Flag–SERCA2a WT or Ad–Flag–SERCA2a-C498S mutant in the presence or absence of *p22^{phox}* siRNA. **l**, Quantification of the Flag–SERCA2a WT protein expression levels in **k** ($n = 12$). **m**, Quantification of the Flag–SERCA2a-C498S mutant protein expression in **k** ($n = 12$). All bar graphs represent the mean ± s.e. Statistical significance was determined using one-way ANOVA with Tukey test (**b**, **c** and **j**) and unpaired Student's *t*-test (two tailed) (**e**, **g**, **l** and **m**).

https://doi.org/10.1038/s44161-025-00699-x

Inhibition of the endogenous interaction between SERCA2a and p22^{phox} leads to SERCA2a oxidation and degradation

We next examined how p22^{phox}–SERCA2a interaction influences SERCA2a stability. We expressed a small fragment of SERCA2a encompassing the p22^{phox}–SERCA2a interaction domain as a minigene in cardiomyocytes to block endogenous p22^{phox}–SERCA2a interaction in vitro. Adenoviruses harboring SERCA2a (334–666) from rat SERCA2a with an N-terminal HA tag was transduced into rat neonatal cardiomyocytes, and the level of SERCA2a was determined by western blotting. Expression of the SERCA2a (334–666)–HA protein resulted in downregulation of endogenous SERCA2a levels in a dose-dependent manner (Extended Data Fig. 5a,b). As observed earlier in this study, immunoprecipitation of the SERCA2a (334–666)–HA protein co-immunoprecipitated endogenous p22^{phox} (Extended Data Fig. 5c), and, as expected, the interaction between endogenous full-length SERCA2a and p22^{phox} was diminished in the presence of SERCA2a (334–666)–HA (Extended Data Fig. 5d). Proteasome inhibition with MG132 partially rescued the lowered SERCA2a protein level

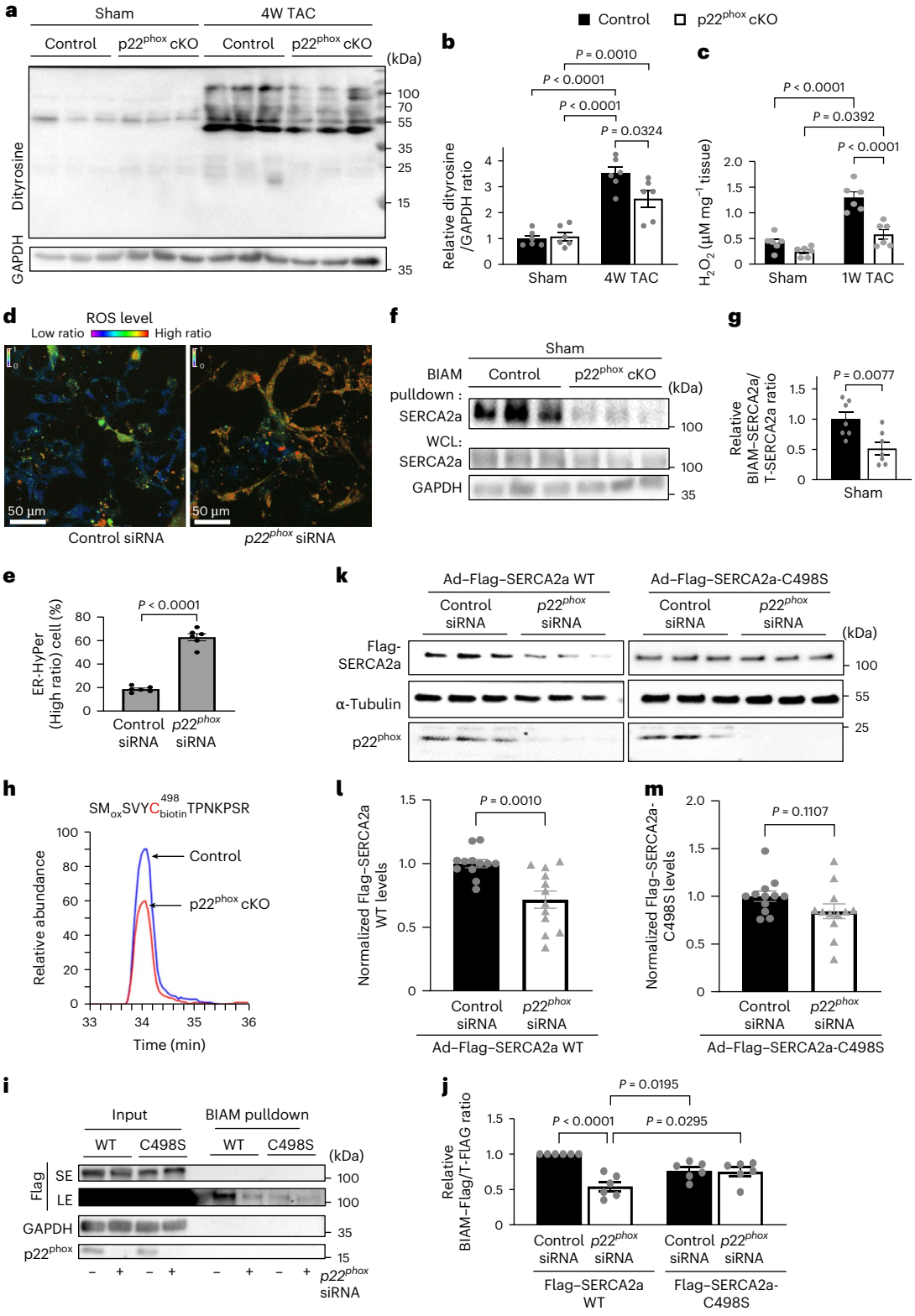

in the presence of SERCA2a (334–666)-HA (Extended Data Fig. 5). To evaluate how the presence of the minigene affects the oxidation status of SERCA2a, BIAM pull-down assays were conducted with cardiomyocytes transduced with either Ad–LacZ or Ad–SERCA2a (334–666)-HA in the presence of MG132. Cardiomyocytes treated with H_2O_2 served as positive control. BIAM–SERCA2a pull-down was lower in the presence of SERCA2a (334–666)-HA than in the presence of LacZ (Extended Data Fig. 5g,h). Furthermore, WT mice injected with AAV9–cTnT–mSERCA2a (333–666)–Flag (minigene) showed lower endogenous SERCA2a levels than those injected with AAV9–cTnT–eGFP (Extended Data Fig. 5i,j). These data suggest that SERCA2a (334–666) binds and sequesters endogenous $p22^{phox}$, thereby leading to increased oxidation and degradation of endogenous SERCA2a protein.

SERCA2a interacts with Smurf1 and Hrd1 E3 ubiquitin ligases under oxidative stress and undergoes proteasomal degradation

In the absence of $p22^{phox}$, SERCA2a undergoes ubiquitination and proteasomal degradation. Therefore, the E3 ubiquitin ligase targeting SERCA2a under oxidative stress was investigated. Smad ubiquitination regulatory factor 1 (Smurf1), a member of the HECT family of E3 ligases, is involved in activin type II receptor-induced degradation of SERCA2a during aging and heart failure[19]. Co-immunoprecipitation with SERCA2a antibody showed that SERCA2a interacts with Smurf1 at baseline, and this interaction is enhanced under H_2O_2-induced oxidative stress (Supplementary Fig. 4a). Interestingly, immunoprecipitation of HA-tagged ubiquitin also showed enhanced Smurf1 association with SERCA2a under oxidative stress (Supplementary Fig. 4a). The results also show that Smurf1 is more highly ubiquitinated under oxidative stress (Supplementary Fig. 4a), probably owing to autoubiquitination, which is known to take place in HECT type E3 ubiquitin ligases[20]. Knockdown of Smurf1 using siRNA partially rescued the H_2O_2-mediated downregulation of SERCA2a (Supplementary Fig. 4b,c).

SERCA2 undergoes ER-associated degradation (ERAD)[21]. Therefore, the involvement of HMG-CoA reductase degradation protein 1 (Hrd1), an ERAD-specific RING family E3 ubiquitin ligase[22], in the degradation of SERCA2a was also investigated in this study. Co-immunoprecipitation experiments showed that SERCA2a interacts with Hrd1 and that this interaction is also enhanced in the presence of H_2O_2 (Supplementary Fig. 4d). Knockdown of Hrd1 alleviated H_2O_2-induced downregulation of SERCA2a (Supplementary Fig. 4e,f).

Co-immunoprecipitation assays revealed that SERCA2a interacts with both Smurf1 and Hrd1, with these interactions markedly enhanced in $p22^{phox}$ knockdown cells treated with epoxomicin (Fig. 7a). Knockdown of Smurf1 or Hrd1 independently led to a partial rescue of SERCA2a levels in $p22^{phox}$-deficient cardiomyocytes (Fig. 7b–e). Immunofluorescence showed increased colocalization of SERCA2a and Hrd1 under $p22^{phox}$ knockdown conditions (Fig. 7f,g). In addition, colocalization of SERCA2a, Hrd1 and the 20S proteasome subunit PSMA3 was elevated in the absence of $p22^{phox}$ (Fig. 7h,i). These findings indicate that Smurf1 and Hrd1 mediate proteasomal degradation of SERCA2a in the absence of $p22^{phox}$.

SERCA2a-C498S knock-in mice show cardioprotection under pressure overload

To evaluate the role of SERCA2a Cys498 oxidation in vivo, we generated SERCA2a-C498S knock-in (KI) mice (Supplementary Fig. 5). Calcium transients in cardiomyocytes from WT and SERCA2a-C498S KI mice (heterozygous and homozygous) revealed no significant differences in amplitude (F/F_0), SR calcium content or tau, indicating preserved calcium handling at baseline (Supplementary Fig. 6). Echocardiography confirmed that SERCA2a-C498S KI (homozygous) mice show normal baseline cardiac function and intact cardiac reserve in response to dobutamine (Supplementary Fig. 7a). Following 3 weeks of TAC or sham surgery, both heterozygous and homozygous KI mice showed preserved ejection fraction (Supplementary Fig. 7b,c), reduced hypertrophy (LVW/TL) (Supplementary Fig. 7d), less lung congestion (lung tissue weight (LungW)/TL) (Supplementary Fig. 7e), smaller cardiomyocyte size (Supplementary Fig. 7f,g) and less interstitial fibrosis (Supplementary Fig. 7h,i) compared with WT mice. TAC reduced *RyR2*, *NCX1* and *SERCA2a* mRNA levels across all groups (Supplementary Fig. 7j–l,o), but SERCA2a-C498S KI mice tended to show lower *NCX1* and *SERCA2a* expression than WT mice (Supplementary Fig. 7k,o). TAC-induced increases in the P-PLN/total PLN (T-PLN) ratio were blunted in SERCA2a-C498S KI mice (Supplementary Fig. 7m,n). Notably, SERCA2a protein levels were preserved in both heterozygous and homozygous SERCA2a-C498S KI mice after TAC, suggesting increased protein stability (Supplementary Fig. 7p,q). Co-immunoprecipitation assays showed reduced interaction between SERCA2a and Smurf1/Hrd1 in SERCA2a-C498S KI mice (Supplementary Fig. 8a). In BIAM pull-down assays, TAC reduced BIAM labeling of SERCA2a in WT mice, consistent with oxidation of cysteine thiols, while labeling remained unchanged in SERCA2a-C498S KI mice, indicating protection from Cys498 oxidation (Supplementary Fig. 8b,c). Together, these findings show that oxidation of SERCA2a at Cys498 during pressure overload promotes its degradation, contributing to cardiac dysfunction, and that the C498S mutation confers protective effects by maintaining SERCA2a levels and cardiac function.

$p22^{phox}$ cKO mice with SERCA2a-C498S KI are protected against progression to heart failure under pressure overload

To assess the functional importance of SERCA2a Cys498 oxidation, we crossed SERCA2a-C498S KI mice with $p22^{phox}$ cKO mice, followed by

Fig. 7 | SERCA2a interacts with Smurf1 and Hrd1 E3 ubiquitin ligases under oxidative stress and undergoes proteasomal degradation. a, NRVMs were transfected with control siRNA or *p22^{phox}* siRNA for 48 h and treated with MG132 for 3 h. The cell lysates were immunoprecipitated with either SERCA2a antibody or IgG control antibody and checked by immunoblotting for interaction with Smurf1 or Hrd1 E3 ubiquitin ligases. The immunoblots show enhanced binding of both Smurf1 and Hrd1 E3 ubiquitin ligases with SERCA2a in the absence of $p22^{phox}$. Epoxomicin treatment at baseline also showed SERCA2a interaction with Hrd1 and Smurf1 (performed at least three times independently). **b**–**e**, NRVMs were transfected with control siRNA or *p22^{phox}* siRNA together with Smurf1 or Hrd1 siRNA as indicated for 48 h. Cell lysates were collected and analyzed for protein levels of SERCA2a by immunoblotting. **b**, Representative immunoblots of SERCA2a with GAPDH as loading control. Knockdown of Smurf1 and $p22^{phox}$ is also validated. **c**, Relative SERCA2a protein levels in **b** ($n = 6$). **d**, Representative immunoblots of SERCA2a with GAPDH as loading control. Knockdown of Hrd1 and $p22^{phox}$ is also validated. **e**, Relative SERCA2a protein levels in **c** ($n = 6$). **f**–**h**, NRVMs were transfected with control siRNA or *p22^{phox}* siRNA for 48 h and stained by immunofluorescence. Images were acquired by confocal microscopy. The blue color indicates DAPI (nucleus), green is SERCA2a, red is Hrd1 and yellow is the colocalization channel. **f**, Representative all-channel confocal microscopy images showing colocalization of SERCA2a and Hrd1. **g**, Three-dimensional (3D) fluorescence reconstructed image using IMARIS software after confocal microscopic image acquisition with *z*-stacks. **h**, The quantification of colocalization was calculated as the ratio of the volume of colocalization to the volume of SERCA2a in each cell following IMARIS software analysis ($n = 6$). **i**, Representative immunofluorescence images from control siRNA or *p22^{phox}* siRNA-treated NRVMs stained with DAPI (white: pseudo color), SERCA2a (red), Hrd1 (blue) and PSMA3 (green). Individual channels are shown separately, and the merge channel is shown enlarged. The purple arrows indicate colocalization of SERCA2a with Hrd1, and the white arrows indicate triple colocalization of SERCA2a, Hrd1 and PSMA3. **j**, The quantification of triple colocalization was calculated as the ratio of the volume of triple colocalization to the volume of SERCA2a in each cell following IMARIS software analysis ($n = 5$). All bar graphs represent the mean ± s.e. Statistical significance was determined using one-way ANOVA with Tukey test (**c** and **e**) and unpaired Student's *t*-test (two tailed) (**h** and **j**).

https://doi.org/10.1038/s44161-025-00699-x

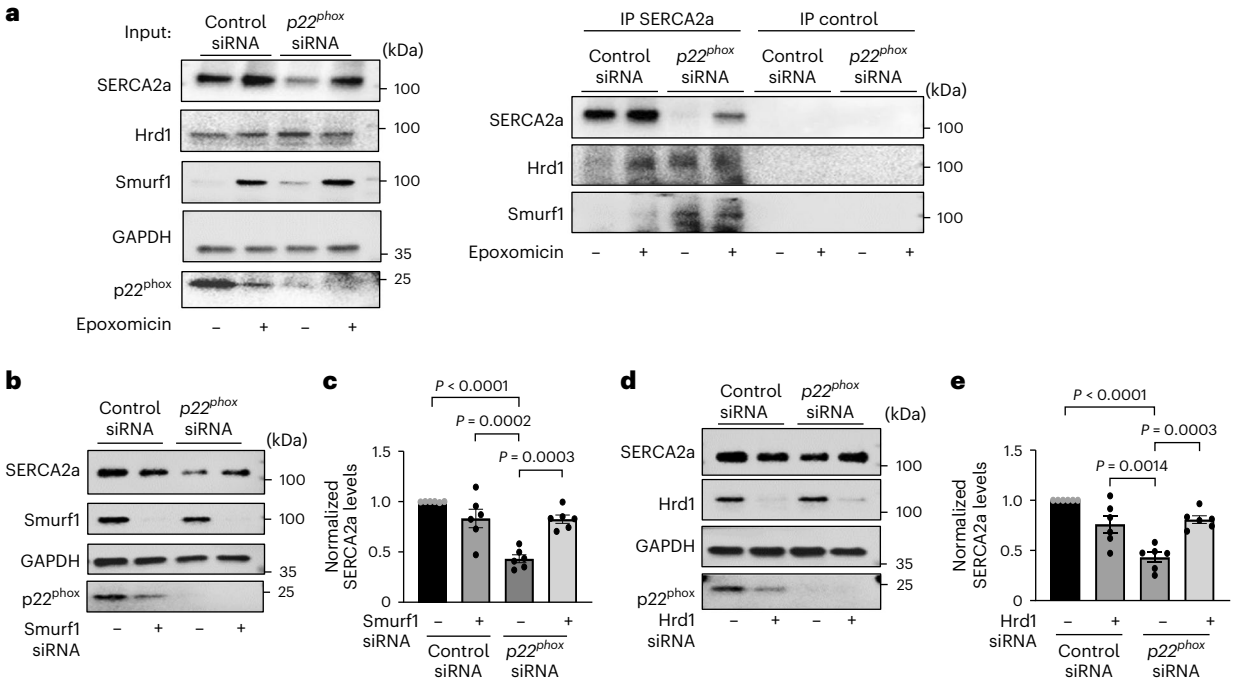

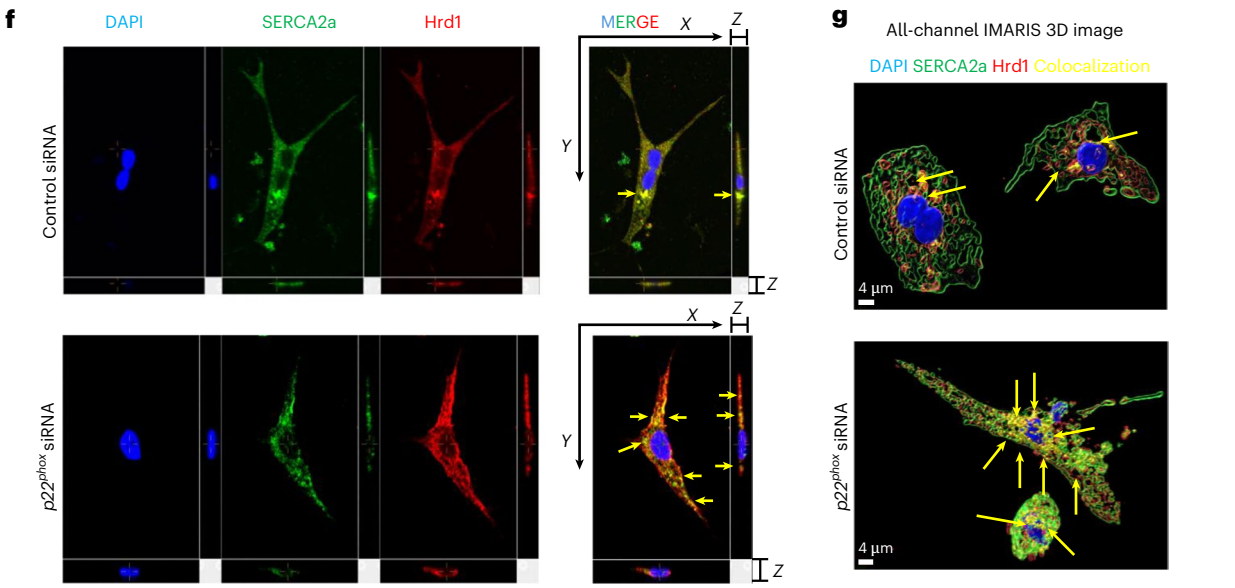

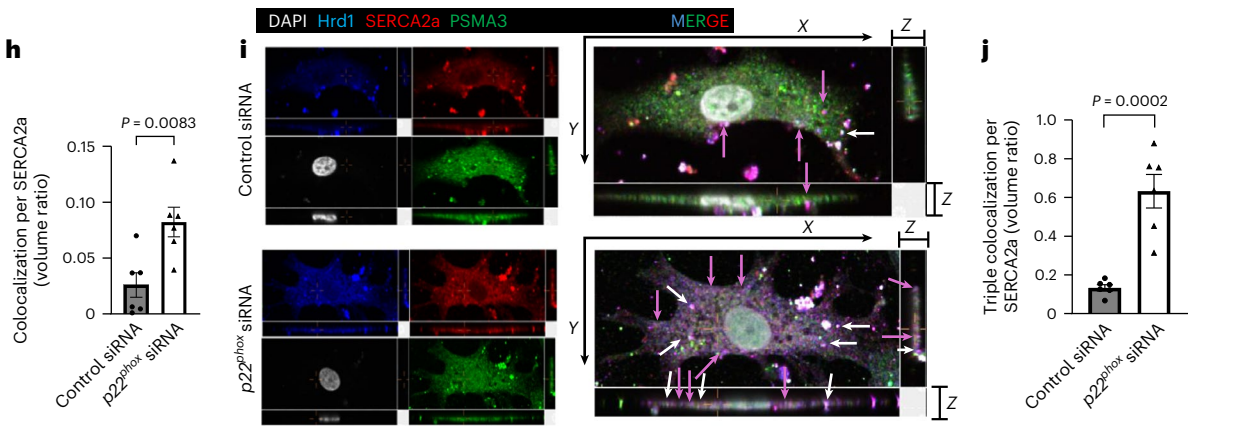

3 weeks of TAC or sham surgery. Consistent with the aforementioned findings, the cross with SERCA2a-C498S KI mice rescued cardiac dysfunction and preserved SERCA2a levels in p22^{phox} cKO mice during pressure overload (Fig. 8 and Supplementary Fig. 9). The cross with heterozygous SERCA2a-C498S KI mice restored LVEF, reduced the LVW/TL and lung W/TL ratios (Fig. 8a–d) and mitigated fibrosis and cardiomyocyte hypertrophy (Supplementary Fig. 9a–d) in p22^{phox} cKO mice. SERCA2a protein levels were significantly higher in p22^{phox} cKO plus SERCA2a-C498S KI mice compared with p22^{phox} cKO alone mice in both sham and TAC conditions (Fig. 8e,f). Importantly, the interaction of SERCA2a with Smurf1 and Hrd1, elevated in p22^{phox} cKO mice, was suppressed in the presence of the C498S KI mutation (Supplementary Fig. 9e). Cardiomyocyte contractility was not significantly altered by SERCA2a-C498S KI compared with the control. However, the reduced contractility in p22^{phox} cKO mice was fully restored by their cross with SERCA2a-C498S KI mice both at baseline and during isoproterenol stimulation (Fig. 8g,h). Similarly, calcium transient defects (reduced amplitude and prolonged tau), seen in p22^{phox} cKO cardiomyocytes, were normalized in the presence of SERCA2a-C498S KI, achieving values comparable to those of the wild type (Extended Data Fig. 6a–c). Despite these functional improvements, SERCA2a ATPase activity remained unchanged in WT, p22^{phox} cKO, SERCA2a-C498S KI and double-mutant groups (Supplementary Fig. 9f), suggesting that the protein level, not enzymatic function, is the critical determinant of dysfunction in p22^{phox}-deficient hearts. Collectively, these findings identify Cys498 oxidation as a key regulatory site mediating SERCA2a degradation and cardiac dysfunction in the absence of p22^{phox}.

SERCA2a levels negatively correlate with increased Smurf1 and Hrd1 levels in human heart failure samples

The molecules associated with the degradation of SERCA2a identified in this study were evaluated in human LV samples from donor (healthy) and recipient (dilated cardiomyopathy (DCM) or ischemic cardiomyopathy (ICM)) samples. Immunostaining of human heart samples showed that the level of SERCA2a in the myocardium was significantly lower in failing hearts than in non-failing hearts (Extended Data Fig. 7a,b). Immunoblotting also showed that SERCA2a protein levels were downregulated in cardiomyopathic hearts compared with healthy hearts (Extended Data Fig. 7c,d). In addition, the levels of Smurf1 and Hrd1 were upregulated in cardiomyopathic hearts compared with control hearts (Extended Data Fig. 7e,f).

Discussion

Downregulation and inactivation of SERCA2a are major mechanisms of heart failure[2]. AAV-vector-mediated supplementation of SERCA2a is insufficient for improving cardiac dysfunction in patients[23], suggesting the presence of complex posttranslational mechanisms regulating both the stability and activity of SERCA2a (refs. 4,24). Unexpectedly, our results show that endogenous p22^{phox} protects SERCA2a from oxidation at Cys498, thereby preventing the downregulation of SERCA2a through ubiquitin proteasome-dependent mechanisms without affecting its ATPase activity. Interventions to prevent the oxidation of SERCA2a at Cys498 should prevent the downregulation of SERCA2a during cardiac stress, thereby maintaining cardiac function.

p22^{phox} has four transmembrane helices and is located primarily on the ER membrane[25]. p22^{phox} forms heterodimeric complexes with Nox isoforms and has an essential role in mediating the production of O_2 and H_2O_2 (refs. 26,27). Studies of the effects of loss of p22^{phox} function reported thus far have suggested that all known functions of p22^{phox} are attributed to its ability to form complexes with Nox isoforms[28]. Our unbiased protein–protein interaction analyses showed, however, that p22^{phox} can interact with many proteins, and SERCA2a, a transmembrane protein on the ER membrane, was identified as the most enriched binding partner of p22^{phox}. Furthermore, as SERCA2a rescue alleviated the cardiac dysfunction in p22^{phox} cKO mice, among the multiple p22^{phox}-interacting proteins, SERCA2a appears to have a significant role in mediating the function of p22^{phox} in the heart during pressure overload. Functional analyses have shown that p22^{phox} protects SERCA2a from oxidation and stabilizes it against proteasome degradation. Although the current study highlights the importance of SERCA2a as a binding partner of p22^{phox} during pressure overload, p22^{phox} may also act as a chaperone to stabilize other transmembrane proteins on the ER, thereby contributing to the pathogenesis of diseases through Nox-independent mechanisms. The tissue-specific p22^{phox} KO mice we generated may be useful for identifying additional functionally relevant partners of p22^{phox} in pathophysiological contexts.

p22^{phox} physically interacted with the intracellular N domain of SERCA2a. As the inhibition of the physical interaction between p22^{phox} and SERCA2a by the minigene harboring SERCA2a (334–666) promoted SERCA2a downregulation, mimicking the effect of the loss of p22^{phox} function, we speculate that the physical interaction between p22^{phox} and SERCA2a protects SERCA2a from degradation. As Cys498 is located in the region of SERCA2a that interacts with p22^{phox}, we speculate that the interaction inhibits SERCA2a oxidation at Cys498 either by physically protecting Cys498 from oxidative stress or by recruiting molecules that inhibit oxidation of SERCA2a.

The SERCA2a N-domain is involved in nucleotide binding and enzyme activity[29], and thus, we initially speculated that oxidation of Cys498, located in the middle of the N-domain, may affect the ATPase activity of SERCA2a. However, as the specific ATPase activity of SERCA2a in p22^{phox} cKO mice does not appear to be decreased, oxidation of SERCA2a at Cys498 may not negatively affect the ATPase activity of SERCA2a. The property of SERCA2a oxidation at Cys498 is distinct from that at Cys674, another major cysteine oxidation site, where the activity of SERCA2a is positively affected by glutathionylation[16]. Our results suggest that SERCA2a oxidation at Cys498 promotes the interaction between SERCA2a and E3 ubiquitin ligases, including Smurf1 and Hrd1, which in turn promotes degradation of SERCA2a. The binding

Fig. 8 | p22^{phox} cKO mice with SERCA2a-C498S KI are protected from progression to heart failure under pressure overload. Control (wild type +/+ MHC cre^{+} or p22^{phox} flox/flox/+ cre−), p22^{phox} cKO (flox/flox MHC cre+), SERCA2a-C498S heterozygous knock-in (C498S het KI) and p22^{phox} cKO with SERCA2a-C498S heterozygous knock-in were subjected to sham surgery or transverse aortic constriction (TAC 3W). The mice were then analyzed for hypertrophic response and cardiac function by echocardiography. The heart LV tissues were collected for the indicated analyses. **a**, Representative echocardiographs from control, p22^{phox} cKO, SERCA2a-C498S heterozygous knock-in and p22^{phox} cKO with SERCA2a-C498S heterozygous knock-in mice after sham surgery or TAC 3W. **b**, LVEF (%) (sham: $n = 6, 7, 9, 7$; TAC: $n = 7, 6, 7, 7$). **c**, LVW/TL ratio (sham: $n = 7, 5, 8, 5$; TAC: $n = 5, 7, 7, 7$). **d**, Lung W/TL ratio ($n = 7$). **e**, The heart LV tissue of the mice that were subjected to sham or TAC 3W was analyzed by western blotting for protein levels of SERCA2a, with GAPDH as loading control. The figure shows representative immunoblots of SERCA2a with GAPDH as loading control from control and p22^{phox} cKO mice with wild type or C498S mutant SERCA2a. **f**, Quantification of SERCA2a levels with respect to GAPDH in **e** ($n = 6$). **g**,**h**, Cardiomyocyte contractility was assessed in isolated cardiomyocytes from the indicated groups under NT solution and isoproterenol (1 μM) (Iso)-stimulated conditions. For each group, four mice and the specified number of cells per mouse were recorded and summarized. **g**, Representative cell shortening calculated as a percentage with electrical stimulation (3 s duration) indicated with arrows. **h**, Quantification graph of the percentage cardiomyocyte shortening in **g** (from left to right, $n = 6, 6, 4, 6$; $n = 5, 5, 4, 6$; $n = 6, 4, 5, 11$; $n = 9, 7, 6, 5$; $n = 6, 6, 3, 3$; $n = 5, 6, 3, 4$; $n = 7, 8, 8, 5$; $n = 7, 7, 8, 8$). The data points from cells of each mouse are represented by colored dots (black, blue, brown and black empty). All bar graphs represent the mean ± s.e. Statistical significance was determined with one-way ANOVA with Tukey test (**b**–**d** and **f**). Statistical analysis was conducted using the nested *t*-test (two tailed) (**h**) and hierarchical clustering analysis and the dendrogram is provided in the source data.

https://doi.org/10.1038/s44161-025-00699-x

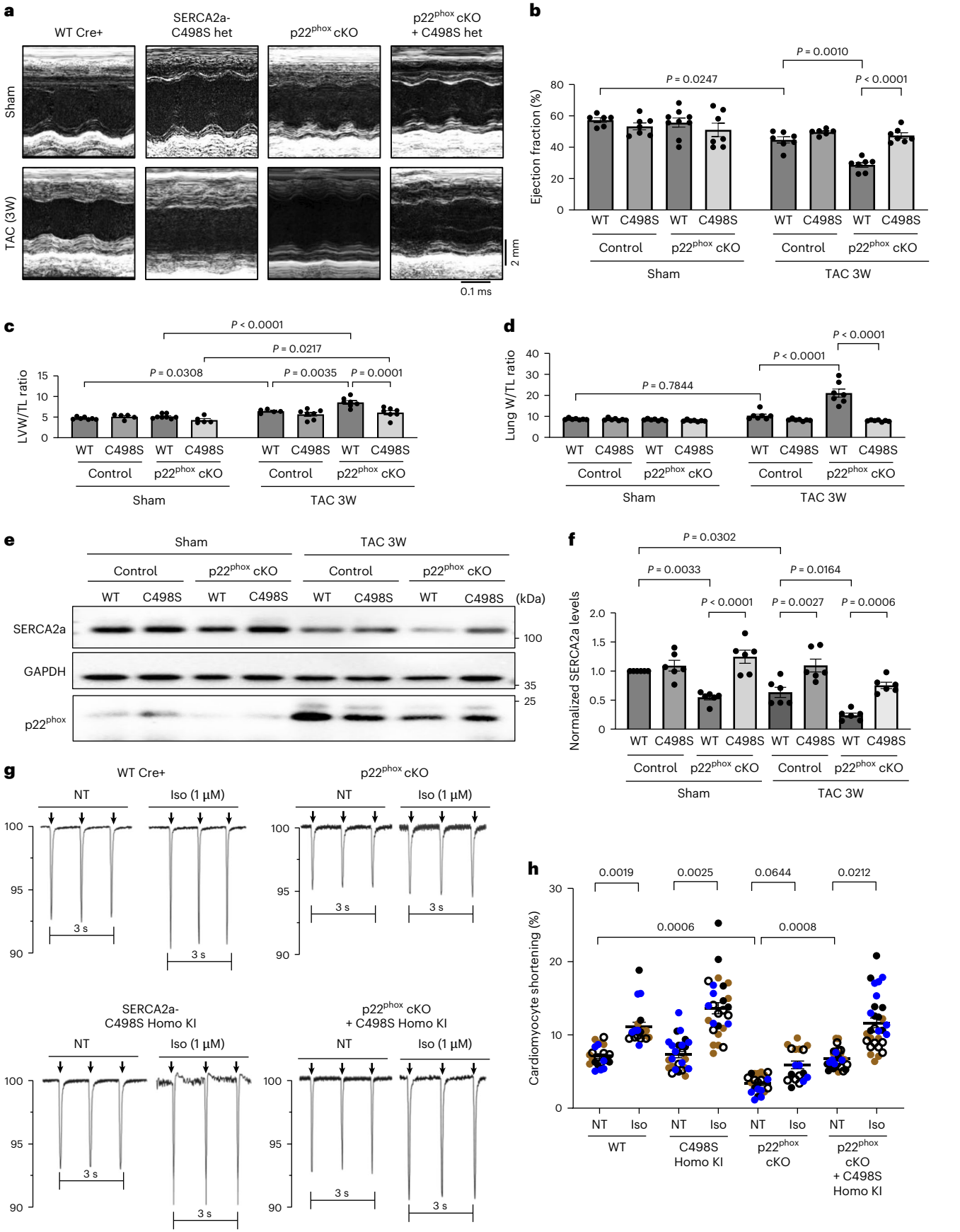

between E3 ligases and substrates is often regulated by posttranslational modification of the substrates, including phosphorylation, hydroxylation, acetylation, glycosylation and SUMOylation[30,31]. Our results show that the mutation of SERCA2a at Cys498 to serine negatively regulates the interaction between E3 ligases and SERCA2a in the presence of oxidative stress, thereby stimulating SERCA2a downregulation. Although further experimentation, including an in vitro direct protein–protein interaction assay with recombinant proteins, needs to be conducted, our results strongly suggest that cysteine oxidation of the substrate regulates the interaction between E3 ligases and the substrate. It has been shown that cysteine oxidation of either E3 ligases or scaffolding proteins affects ubiquitin proteasome protein degradation[32,33]. However, to our knowledge, the SERCA2a–E3 ligase interaction is unique in that cysteine oxidation on the substrate side controls the interaction.

Among the ubiquitin E3 ligases whose interaction with SERCA2a is increased by Cys498 oxidation, Hrd1 belongs to E3 ligases involved in the ERAD, the process mediating the proteasome-dependent degradation of ER proteins[34]. The ERAD machinery facilitates the efficient degradation of ER proteins in the presence of stress, and thus, the ERAD often has an adaptive and physiological role[34]. Thus, the fact that SERCA2a uses ERAD for its degradation and that it may negatively impact cardiac function during stress are interesting. Further investigation is needed to elucidate the functional significance of the Hrd1-mediated degradation of SERCA2a. Smurf1, another E3 ligase, also has an important role in mediating the degradation of SERCA2a (ref. 19). Whether Hrd1 and Smurf1 have redundant roles or mediate distinct stress-specific roles remains to be elucidated.

$p22^{phox}$ inhibits SERCA2a oxidation at Cys498. This was unexpected in that $p22^{phox}$ is involved in the Nox-mediated production of ROS[25] and that the bulk level of oxidative stress in the heart homogenate in $p22^{phox}$ cKO mice was lower than in WT mice in the presence of pressure overload, consistent with the involvement of the Nox–$p22^{phox}$ complex in mediating oxidative stress during pressure overload. Interestingly, $p22^{phox}$ cKO mice showed increases in H_2O_2 in the ER, as evaluated with ER-targeted Hyper. Thus, $p22^{phox}$ protects SERCA2a from oxidative stress in the local compartment of the ER. We have shown previously that a lack of HAX-1, an ER/SR-associated protein, also increases oxidative stress in an ER-specific manner[12]. Thus, it is possible that ER-associated proteins have an intrinsic ability to suppress oxidative stress in the ER. We speculate that a lack of endogenous ER proteins, such as $p22^{phox}$, induces ER stress and protein misfolding, which is often accompanied by oxidative stress[35]. It is also possible that $p22^{phox}$ may recruit antioxidants, such as thioredoxin-like molecules, to the proximity of the ER proteins to alleviate oxidation. Further investigation is required to elucidate the underlying molecular mechanisms.

The level of $p22^{phox}$ is increased in response to pressure overload and in some forms of cardiomyopathy. As genetic downregulation of $p22^{phox}$ exacerbates heart failure during pressure overload, upregulation of $p22^{phox}$ during pressure overload appears to be an adaptive mechanism. As the upregulation of $p22^{phox}$ is attenuated during the chronic phase of pressure overload and the upregulation is not observed in some forms of heart failure in humans, it is possible that the decline in $p22^{phox}$ may contribute to the inhibition of SERCA2a in the failing heart. It has been shown that $p22^{phox}$ is downregulated during hypoxia, in which downregulation of SERCA2a is also observed[36]. Currently, the molecular mechanisms through which expression of $p22^{phox}$ is controlled during stress are unknown. An investigation of the mechanisms controlling the level of $p22^{phox}$ may lead to the discovery of interventions allowing the stabilization of SERCA2a during heart failure.

Although the function of SERCA2a is consistently inhibited in human failing hearts, how SERCA2a is inhibited appears complex and context dependent. Whether or not SERCA2a is downregulated at the protein level is controversial[37–44]. Furthermore, posttranslational modifications of SERCA2a also affect the activity of SERCA2a (refs. 4,24). Thus, to effectively restore the function of SERCA2a during heart failure, it is important to know how the level and the activity of SERCA2a are modified and identify the underlying mechanisms. Our results suggest that oxidation of SERCA2a at C498 increases proteasomal degradation of SERCA2a without inhibiting its ATPase activity. Thus, interventions to alleviate C498 oxidation and block Smurf1- or Hrd1-mediated degradation of SERCA2a may be of value in preventing SERCA2a downregulation during heart failure. Identification of other mechanisms regulating the activity of SERCA2a should further contribute to achieving more efficient rescue of SERCA2a downregulation during heart failure.

Some experimental limitations are noted. First, the downregulation of $p22^{phox}$ increased oxidation of SERCA2a at multiple cysteines. We focused on oxidation of Cys498 as it is oxidized most efficiently in vitro. The functional significance of SERCA2a oxidation at other cysteines needs to be clarified. Second, the molecular mechanism through which SERCA2a is oxidized at Cys498 remains unexplored. In particular, we are investigating the molecular mechanisms through which oxidative stress is regulated in the ER/SR and how $p22^{phox}$ interacts with these mechanisms. Third, during muscle contraction, mouse muscle cells typically release approximately 90% of their SR calcium stores, whereas human muscle cells release about 70% (ref. 45). Thus, the extent to which SERCA2a oxidation at Cys498 affects overall excitation–contraction (EC) coupling may differ between mice and humans. Fourth, regulation of oxidative stress in the heart is greatly affected by the genetic background. For example, oxidative stress is generally higher in C57BL/6N mice than in the C57BL/6J mice used in this study[46]. Thus, whether the $p22^{phox}$-mediated local regulation of oxidative stress in the ER also differs among mouse strains remains to be tested.

In summary, our study has identified a mechanism by which oxidation and degradation of SERCA2a are mediated in the heart. The knowledge obtained from our study should be useful for designing molecular interventions to maintain the function of SERCA2a during cardiac stress and heart failure.

Methods

Human samples

The samples from explanted hearts used in this study (Fig. 1a and Extended Data Fig. 7c) were obtained from donors and patients who had undergone heart transplantation at Taipei Veterans General Hospital (VGH), Taiwan (Supplementary Tables 1 and 6). The study was approved by the Ethics Committee of Taipei VGH, and all specimens were from the residual sample bank, Taipei VGH. The Institutional Review Board (IRB) number is Taipei VGH IRB number 2018-05-006BC. The human tissue immunofluorescence data in Extended Data Fig. 7a,b was collected at Nara Medical University, Japan (Supplementary Table 5). The study protocols were approved by the Nara Medical University Ethics Committee, G107, and followed the 1975 Declaration of Helsinki guidelines. Written informed consent to collect tissue, conduct research and publish results anonymously was obtained from all participants and/or their legal guardians before the collection.

Mouse models

We generated $p22^{phox}$ knockout ($p22^{phox}$cKO) mice using lox-P and homologous recombination strategies (Supplementary Fig. 2a,b). These mice were backcrossed into a C57BL/6J background. Cardiac-specific deletion of $p22^{phox}$ was obtained by crossing the mice with α-myosin heavy chain (α-MHC) promoter-driven heterozygous Cre mice (a gift from M.D. Schneider). Age- and sex-matched mice without α-MHC Cre recombinase were used as littermate control mice (control mice). The mice were housed in a temperature-controlled environment within a temperature range of 21–23 °C with 12-h light–dark cycles. All experiments involving animals were approved by the Rutgers New Jersey Medical School's Institutional Animal Care and Use Committee.

Generation of KI mice

We generated SERCA2a-C498A knock-in mice using Crispr-Cas9 genome editing in the C57BL/6J background. Genotype was confirmed using genomic DNA sequencing and PCR analyses. For PCR analysis, the genomic DNA isolated from mice were PCR amplified for the exon 12 of SERCA2a (ATP2a2) using forward primer: AAGGTCTAATGCGTATCTGAGCAG and reverse primer: CTGTTTGACACCAGGAGTCATGG. The PCR condition for these primers are:

Initial denaturation: 94 °C, 3 min (94 °C, 15 s; 68 °C, 60 s) × 35 cycles, and then 4 °C, hold. The Taq polymerase used is Advantage-2 catalog number 639202 from Clontech. A total of 5 µl of the PCR is digested with ScaI restriction enzyme. The Atp2a2-C498S mutated fragment generates two fragments at 210 bp and 132 bp whereas the Atp2a2 wild-type fragment is not cut with ScaI and gives a 342-bp fragment. The knock-in mice were crossed with wild-type C57BL/6J mice five times.

Mass spectrometry analysis

Cardiomyocytes isolated from mouse hearts were lysed with lysis buffer (150 mM NaCl, 50 mM Tris–HCL, 0.5% Triton X-100 and protease inhibitors). The lysates were incubated with recombinant Flag–$p22^{phox}$ (10 µg) and anti-Flag-M2 beads (Sigma-Aldrich) at 4 °C for 4 h. The beads were washed three times with lysis buffer, and Flag–$p22^{phox}$ binding proteins were eluted with 3×FLAG peptide (Sigma). The elutant was subjected to SDS-PAGE. Each gel lane was excised and in-gel trypsin digestion was performed. The resulting peptides were analyzed by LC–MS/MS on a Q Exactive MS instrument (Thermo Scientific)[47,48]. The MS/MS spectra were searched against a Swissprot rat database using the Sequest search engine on the Proteome Discoverer platform (V.2.3). All proteins and peptides were identified with a false discovery rate of less than 1%. The protein relative abundance was calculated based on spectrum counting.

TAC

All animal experiments were conducted in accordance with protocols approved by the Rutgers University Animal Care and Use Committee. The TAC model was used to assess the effect of pressure overload on the development of heart failure in mice. The methods used to impose pressure overload in mice have been described[49]. Male mice at 8–12 weeks of age and fed a normal chow diet were randomly divided into two groups, pressure overload with TAC or sham operation. We focused on male mice in this study. Age- and sex-matched mice were used for the control group. The background of all mice was C57BL/6J. Mice were anesthetized with pentobarbital sodium (60–70 mg kg^{-1}) and mechanically ventilated. The left side of the chest was opened at the second intercostal space. Aortic constriction was performed by ligation of the transverse thoracic aorta between the innominate artery and left common carotid artery with a 27-gauge needle using a 7-0 prolene suture. Sham operation was performed without constricting the aorta. The number of animals used is described in each figure legend. There were no unexpected adverse events during the procedures. All operations and analyses were performed in a blinded manner with regard to the genotype of mice. To measure the aortic pressure gradient across the constriction, high-fidelity micromanometer catheters (1.4 French; Millar Instruments) were used.

Dobutamine stress test

Mice were anesthetized using 12 µl g^{-1} body weight of 2.5% avertin (Sigma-Aldrich) and prepared for cardiac catheterization[50]. The dobutamine infusion was administered via jugular vein cannulation with a PE-10 tube attached to an infusion pump (catalog number BTPE-10). Dobutamine infusion (10 ng $µl^{-1}$) was set up for ramp infusion in a step-to-step format with an increase of 10 µl min^{-1} for each step, for 3 steps. The data were acquired using LabChartPro 7 software, and the ejection fraction was analyzed and expressed relative to wild-type mice at dobutamine infusion rates of 0, 4, 8 and 12 ng g^{-1} min^{-1}.

Echocardiography

Mice were anesthetized using 12 µl g^{-1} body weight of 2.5% avertin (Sigma-Aldrich), and echocardiography was performed using ultrasound (Visualsonics Vevo 770). A 30-MHz linear ultrasound transducer was used. Two-dimensional guided M-mode measurements of LV internal diameter were obtained from at least three beats and then averaged. LV end-diastolic dimension (LVEDD) was measured at the time of the apparent maximal LV diastolic dimension, and LV end-systolic dimension (LVESD) was measured at the time of the most anterior systolic excursion of the posterior wall. LVEF was calculated as follows: ejection fraction = $((LVEDD)^3 - (LVESD)^3)/(LVEDD)^3 \times 100$. For all mouse experiments, data analysis was conducted in a blinded manner.

Recombinant proteins

The bacterial expression vector for glutathione *S*-transferase (GST)-fused $p22^{phox}$-full-length was generated by insertion of mouse $p22^{phox}$ cDNA amplified by PCR into the pCold-GST-vector. The BL21 *Escherichia coli* strain was transformed with pCold-GST-$p22^{phox}$-full length. The *E. coli* was cultured in 3 ml LB medium containing ampicillin overnight at 37 °C, and then transferred to 250 mL LB medium containing ampicillin. Protein expression was induced by addition of 1 mM isopropylthio-β-galactoside. After overnight culture at 15 °C, the *E. coli* were lysed in lysis buffer (1% Triton X-100 and 1 mM DTT in phosphate-buffered saline (PBS)) with sonication. The lysate was incubated with 0.5 ml glutathione-sepharose 4B (GE Healthcare) for 1 h at 4 °C. The sepharose was washed 3 times with 5 ml lysis buffer and then suspended with 1 ml cleavage buffer (20 mM Tris (pH 7); 150 mM NaCl; 1 mM DTT). Recombinant SERCA2a protein was purchased from Lifespan Biosciences (G27566).

Adenovirus constructs

Recombinant adenovirus vectors for overexpression were constructed, propagated and titered as previously described[51]. Briefly, pBHGloxΔE1,3 Cre plasmid (Microbix) was co-transfected with pDC316 shuttle vector (Microbix) harboring the gene of interest into HEK293 cells using Lipofectamine 2000 (Life Technologies). An in-house-generated adenovirus harboring β-galactosidase (Ad–LacZ) was used as a control.

Primary culture of neonatal rat CMs

Primary cultures of CMs were prepared from 1-day-old Charles River Laboratories (Crl)/Wistar Institute (WI) BR-Wistar rats (both sexes) (Harlan Laboratories) and maintained in culture. A cardiomyocyte-rich fraction was obtained by centrifugation through a discontinuous Percoll gradient. CMs were cultured in complete medium containing Dulbecco's modified Eagle's medium/F-12 supplemented with 5% horse serum, 4 mg ml^{-1} transferrin, 0.7 ng ml^{-1} sodium selenite, 2 g l^{-1} bovine serum albumin (fraction V), 3 mM pyruvate, 15 mM Hepes (pH 7.1), 100 mM ascorbate, 100 mg l^{-1} ampicillin, 5 mg l^{-1} linoleic acid and 100 mM 5-bromo-2′-deoxyuridine (Sigma-Aldrich). Culture dishes were coated with 0.3% gelatin.

Isolation and culture of adult mouse CMs

Isolation and culture of adult mouse CMs were conducted according to the protocol previously described[52].

Tissue-released H_2O_2 measurement

The tissue H_2O_2 was measured with the Amplex Red Hydrogen Peroxide/peroxidase Assay Kit (Molecular Probes, Invitrogen reference A22188). The heart tissue was freshly collected and sectioned on a matrix block with PBS-wetted fresh blades. Each section was immediately submerged into 200 µl of Amplex Red reagent (100 µM) and placed in a 24-well plate. The plate was incubated at 37 °C for 30 min (protected from light). After incubation, 2 × 100 µl of the incubated reagent from the tissue section was taken for fluorescence readings

measured at 530 nm excitation and 590 nm emission. The amount of H_2O_2 released from the tissue sections was estimated against known H_2O_2 standards, and the values were normalized with the weight of the section in mg. The values obtained from all the sections of one heart were averaged to represent one data point on the graph.

ER-HyPer and Mito-HyPer confocal imaging

Adenoviruses encoding the HyPer fluorescence H_2O_2 sensor with endoplasmic reticulum localization signal or mitochondria localization signal were expressed in neonatal rat cardiomyocytes as described[53]. Following transfection with control siRNA and *p22*^{phox} siRNA, the cells were imaged live using confocal microscopy with excitation at 457 nm and emission at 514 nm. The ratiometric (514 nm/457 nm) images were generated with a 2-fold threshold. The scale of the ratiometric image ranges from 0 (low H_2O_2) to 2-fold (high H_2O_2), with default color indicators.

SERCA2a ATPase assays

The cardiac SR fraction was isolated as previously described[54]. Briefly, heart tissue is perfused with 0.9% saline containing 500 µM EDTA (the buffer should not contain phosphates). The fresh heart tissue or frozen heart tissue was homogenized using a Dounce homogenizer in 0.25 M sucrose (with protease inhibitors). The lysate is centrifuged at 500 *g* for 10 min at 4 °C. The resulting supernatant is centrifuged at 10,000 *g* for 10 min at 4 °C. The resulting supernatant is centrifuged at 30,000 *g* for 1.5 h at 4 °C. The pellet fraction is the SR fraction that is estimated for the protein amount and used for ATPase assay after dissolving the pellet in 0.25 M sucrose (with protease inhibitors).

SR-associated SERCA2a ATPase activity was determined using a colorimetric method[55]. The production of phosphate that is proportional to the SERCA activity was measured using an ATPase activity assay kit (MAK113, Sigma-Aldrich), following the manufacturer's protocol. Briefly, SR protein (1 µg) after SR fractionation as above was incubated with calcium chloride (2 µM) with and without thapsigargin (75 µM) along with 1 mM ATP and incubated at 37 °C for 30 min. The reaction was stopped by the addition of the malachite green reagent provided in the kit, which forms a stable dark green color with free phosphate released by the reaction that can be colorimetrically measured at 620 nm. The SERCA2a ATPase activity of the SR fractions was calculated as the difference between values without and with thapsigargin. This value was again normalized to the SERCA2a levels in the respective SR fractions as determined by western blotting, and the relative activity was analyzed with respect to the wild-type SR fraction.

Antibodies and reagents

The primary antibodies used in this study were as follows: p22^{phox} (Abcam: ab191512 and Invitrogen: PA5-75653), Flag (Sigma-Aldrich:1804), GAPDH (Cell Signaling: 2118), α-tubulin (Sigma-Aldrich: 6199), SERCA2a (Cell Signaling: 4388S for western blot, Abcam: 150435 for immunoprecipitation), T-PLN (Cell Signaling: 14562), phospho-PLN (Ser16/17) (Cell Signaling: 8496), Smurf1 (Sigma-Aldrich: WH0057154M1), Hrd1 (Proteintech: 67488-1), PSMA3 (Cell Signaling: 12446S for western blotting and Proteintech: 11887-1 for immunofluorescence), NOX2/*gp91*^{phox} (abcam: 129068) and NOX4 (Proteintech: 14347-1-AP). The secondary antibodies used in this study were as follows: anti-rabbit IgG HRP-linked antibody (Cell Signaling: 7074) and anti-mouse IgG HRP-linked antibody (Cell Signaling: 7076).

The siRNAs used in this study are as follows: rat *p22*^{phox} siRNA (identifier (ID): s236253), rat Smurf1 siRNA (ID: s234756), rat Hrd1 siRNA (ID: s167862) rat Psma3 siRNA (ID: s131972), rat Nox4 siRNA(ID: 190243/190244/190245 and 55016) and rat ATP2A2 (SERCA2a) siRNA (ID: 160790) (Silencer Select siRNA from Thermo Fisher Scientific, Invitrogen). The Transfection reagent used is lipofectamine RNAiMAX (Invitrogen: 13778075).

Quantitative RT-PCR

Total RNA was extracted from mouse hearts using TRIzol (Invitrogen). Total RNA was converted to cDNA using PrimeScript RT Master Mix (Takara). The following oligonucleotide primers were used in this study: p22^{phox}, sense (5′- GTATTTCGGCGCCTAC TCTATC-3′) and antisense (5′-GTCAGGTACTTCTGTCCACATC-3′); 18S, sense (5′-AGTCCCTGCCCTTTGTACACA-3′) and antisense (5′-CGATCCGAGGGCCTCACTA-3′); SERCA2a, sense (5′-CATCAGTATG ACGGGCTTGTAG-3′) and antisense (5′-CTCGGTAGCTTCTCCAA CTTTC-3′); NCX, sense (5′-AGTCTCCCACCCAATGTTTC-3′) and antisense (5′-CTCCTGTTTCTGCCTCTGTATC-3′); PLN, sense (5′-TATCAGGAGAGCCTCCACTATT-3′) and antisense (5′-CAGATCAG CAGCAGACATATCA-3′); and RyR, sense (5′-CTTCTGTGAGGACACCATCT TT-3′) and antisense (5′-CCTCTCCTTCTCACTCTCTTCT-3′). Data were normalized with the RT-PCR result for GAPDH. Quantitative RT-PCR was performed on the CFX 96 RealTime PCR Detection System (Bio-Rad). The Ct value determined using CFX Manager Software (version 2.0, Bio-Rad) for all samples was normalized to GAPDH, and the relative fold change was computed by the comparative Ct (ΔΔCt) method.

Immunoblot analysis

Heart homogenates and CM lysates were prepared in RIPA lysis buffer containing protease and phosphatase inhibitors (Sigma-Aldrich). Equal amounts of samples were separated by SDS-PAGE and transferred onto PVDF membranes. The antibodies used were as described above. The regions containing proteins were visualized by the enhanced chemiluminescence system (ECL Prime Western Blotting Detection Reagent, GE Healthcare). Densitometric analyses were performed with the ImageJ software.

Histological analysis

The heart tissue was washed with PBS, fixed with 4% phosphate-buffered paraformaldehyde, embedded in paraffin and cut into 10-µm-thick sections. Serial sections of the heart were stained with wheat germ agglutinin for analysis of the CM CSA and Picrosirius Red for analysis of myocardial fibrosis. CSA was obtained by tracing the outlines of 100–200 random CMs with a clear nuclear image from the LV. These analyses were performed in a blinded manner using a fluorescence microscope (Eclipse E800, Nikon) and ImageJ software (NIH).

Cardiomyocyte isolation

Left ventricular myocytes were enzymatically isolated from mouse hearts as previously described[56]. Briefly, mice were deeply anesthetized with isoflurane before hearts were removed and perfused in Langendorff fashion at 37 °C with Ca^{2+}-free Tyrode's solution (in mM: 136 NaCl, 5.4 KCl, 1 $MgCl_2$, 0.33 NaH_2PO_4, 10 glucose and 10 HEPES, pH 7.4) containing 0.2 mg ml^{-1} Liberase TL Research Grade (number 05401020001; Sigma-Aldrich, Roche) for 10–12 min. The enzyme solution was then washed out, and the hearts were transferred from the Langendorff apparatus to petri dishes. Left ventricles were gently teased apart with forceps. The Ca^{2+} concentration was gradually increased to 1.0 mM. Finally, the cell suspension was filtered through a 200-µm nylon mesh. Myocytes were stored at room temperature and used within 8 h after isolation for cell shortening assays or intracellular Ca^{2+} transient measurements.

Cardiomyocyte contraction or single-cell shortening assay

Adult mouse ventricular cardiomyocytes were isolated via retrograde Langendorff perfusion using enzymatic digestion as described above. Myocytes were placed in a heated chamber (37 °C) and superfused with normal Tyrode's (NT) solution on an inverted microscope (Nikon Eclipse TE200) and were subjected to 1-Hz field-pacing using a stimulator (Grass Instruments). Changes in cell length were monitored by a video-based edge detection system (Crescent Electronics). Contraction traces were

recorded and analyzed using commercially available pCLAMP10 software (Molecular Devices). Single-cell shortening was calculated as a percentage of shortening from the baseline cell length in the relaxed state. A minimum of five cells per mouse were recorded, and the median value of at least three consecutive contractions per cell was used for the analysis.

Intracellular Ca^{2+} transient measurement

This method has been described previously[56]. In brief, ventricular myocytes were incubated with 4 µm Fluo-4 AM (Invitrogen by Thermo Fisher Scientific) for 40 min. After washing and de-esterification (30 min), the cells were transferred to a heated chamber (37 °C) on a Nikon Eclipse TE200 inverted microscope (Nikon) with a Fluor ×40 oil objective lens (numerical aperture 1.3). The fluorescence (excitation/emission: 485/530 nm) was recorded with a spatial resolution of 500 × 400 pixels at 50 frames per second by an iXon Charge-Coupled Device (CCD) camera (Andor Technology) operated with Imaging Workbench software (INDEC BioSystems). Ca^{2+} fluorescence intensity was expressed as the ratio F/F_0 (fluorescence (F) over the baseline diastolic fluorescence (F_0)). The amplitude of the 10 mmol l^{-1} caffeine-induced Ca^{2+} transient was used as a measure of total SR Ca^{2+} content. Fractional SR Ca^{2+} release was calculated by dividing the height of the last twitch transient by the height of the caffeine transient. The tau values were obtained by using the curve-fitting function (nonlinear exponential decay 1 function) of the Origin 2025 software after carefully selecting the decay phase fluorescence and time values of individual peaks.

PLA

PLA technology allows the detection of interactions between endogenous proteins, based on the detection of protein proximity. PLA was carried out with Duolink In Situ Detection Reagents (Sigma-Aldrich). In brief, myocytes were washed, blocked and then incubated with anti-$p22^{phox}$ and anti-SERCA2a primary antibodies for 2 h at room temperature. After they were washed, the myocytes were incubated with Duolink PLA MINUS and PLUS probes for 1 h at 37 °C. A Duolink in situ detection kit was used for ligation and amplification. DAPI was used to stain the nucleus. The images were captured using a microscope, and red spots indicate the interaction between $p22^{phox}$ and SERCA2a.

Immunofluorescence and confocal microscopy

NRCMs were plated on 1% gelatin-coated glass-bottom 35-mm dishes. The cells were transfected with control siRNA or *p22^phox^* siRNA for 48 h. After transfection, the cells were washed with PBS and fixed in 4% paraformaldehyde for 10 min at room temperature. The fixed cells were further washed with PBS three times, and the cells were permeabilized with 0.5% Triton X-100 in PBS and blocked with 5% BSA in 0.5% Triton X-100 for 1 h at room temperature. Primary antibodies (SERCA2a, Hrd1 and PSMA3 at dilution 1:200) were diluted in 5% BSA–0.5% Triton X-100 in PBS and incubated overnight at 4 °C. After three PBS washes, the respective fluorescent secondary antibodies (1:1,000) were added and incubated for 1 h at room temperature (in the dark). The cells were washed three times with PBS and mounted with Fluoromount-G containing DAPI. Slides were imaged using a Nikon A1 confocal microscope fitted with a ×63 oil-immersion lens, and images were analyzed with Imaris software (version 10.0.1).

Immunoprecipitation

CMs were lysed with lysis buffer containing 50 mM Tris–HCl (pH 7.4), 150 mM NaCl, 0.5% Triton-X 100, Protease Inhibitor Cocktail (Sigma-Aldrich) and Phosphatase Inhibitor Cocktail (Sigma-Aldrich). Samples were incubated with anti-Flag agarose beads (Sigma-Aldrich) for at least 2 h at 4 °C. After immunoprecipitation, the samples were washed with lysis buffer five times and eluted with 2× SDS sample buffer.

In vitro binding assays

Recombinant GST-SERCA2a proteins were incubated with or without recombinant Flag–$p22^{phox}$ in lysis buffer containing 50 mM Tris–HCl (pH 7.4), 150 mM NaCl and 0.1% Triton-X 100 with rotation for 2 h at 4 °C, followed by pull-down with anti-Flag agarose. After washing seven times with lysis buffer, proteins were eluted with 2× SDS sample buffer.

Cycloheximide chase assays

NRCMs were transduced with adenoviruses that encode WT SERCA2a–Flag or C498S SERCA2a–Flag together with LacZ or *p22^phox^* shRNA. At 48 h after transduction, the cells were treated with epoxomicin (50 µM) or DMSO (vehicle control) at the 0-h timepoint in the respective groups. Cycloheximide (at 15 µg ml^{-1} final concentration) was added at time T_0, T_3, T_6 and T_9 at regular 3-h intervals, and cells were collected at T_9, resulting in the following groups: 0 h (T_9), 3 h (T_6), 6 h (T_3) and 9 h (T_0). The cell lysates were analyzed by western blotting for the expression levels of Flag-tagged SERCA2a WT or C498S. The data shown in the graphs were calculated as the percentage of the normalized Flag to GAPDH ratio at T_0 of the respective comparisons.

BIAM labeling

Free reactive thiols in SERCA2a were labeled with BIAM (Sigma-Aldrich). Frozen ventricles were homogenized in lysis buffer that contained protease inhibitors, and 100 µM BIAM. The homogenate was centrifuged at 16,560 *g*. BIAM-labeled proteins were separated from the total protein using streptavidin–agarose beads (Sigma-Aldrich) with rotation for 4 h at 4 °C. The samples were washed with lysis buffer three times and eluted with 2× SDS sample buffer. BIAM-labeled SERCA2a was detected by western blot analysis as described above.

Statistical analysis

All data points were obtained from independent experiment samples. In the bar graphs, individual data values (n) are represented by symbols. Each experiment was repeated at least five or six times. All values for continuous data are expressed as mean ± s.e.m. Statistical analyses were carried out by two-tailed unpaired Student's t-test for two groups or one-way ANOVA followed by Tukey's post hoc analysis for three groups or more, assuming independent variables, normal distribution and equal variance of samples. Categorical variables were compared using Fisher's exact test. $P < 0.05$ was taken as statistically significant. Statistical parameters can be found in the figure legends. Statistical analyses were preformed and graphs were prepared using GraphPad Prism 10 (GraphPad software). The calcium transient studies in isolated cardiomyocytes were analyzed using the in-built nested analysis of GraphPad Prism (10.4.2). A hierarchical clustering dendrogram was generated using Ward's method and Euclidean distance, visualized via ChatGPT (OpenAI).

Reporting summary

Further information on research design is available in the Nature Portfolio Reporting Summary linked to this article.

Data availability

The data that support the findings of the study, including statistical analyses, and reagents used are available in the article and Supplementary Information. The result of the proteomic analysis is shown in Supplementary Table 4. The mouse lines generated in this study, including $p22^{phox}$ *flox/flox* mice and SERCA2a-C498S KI mice, may be requested from the corresponding author and can be shared with the scientific community upon reasonable request, depending on the availability of breeder mice, via a material transfer agreement. Source data are provided with this paper.

References

1. Luo, W. et al. Phospholamban gene dosage effects in the mammalian heart. *Circ. Res.* **78**, 839–847 (1996).
2. Hajjar, R. J., Schmidt, U., Kang, J. X., Matsui, T. & Rosenzweig, A. Adenoviral gene transfer of phospholamban in isolated rat cardiomyocytes. Rescue effects by concomitant gene transfer of sarcoplasmic reticulum Ca^{2+}-ATPase. *Circ. Res.* **81**, 145–153 (1997).
3. del Monte, F. et al. Improvement in survival and cardiac metabolism after gene transfer of sarcoplasmic reticulum Ca^{2+}-ATPase in a rat model of heart failure. *Circulation* **104**, 1424–1429 (2001).
4. Yla-Herttuala, S. Gene therapy for heart failure: back to the bench. *Mol. Ther.* **23**, 1551–1552 (2015).
5. Tsutsui, H., Kinugawa, S. & Matsushima, S. Oxidative stress and heart failure. *Am. J. Physiol. Heart Circ. Physiol.* **301**, H2181–H2190 (2011).
6. Nagarajan, N., Oka, S. & Sadoshima, J. Modulation of signaling mechanisms in the heart by thioredoxin 1. *Free Radic. Biol. Med.* **109**, 125–131 (2017).
7. Ago, T. et al. A redox-dependent pathway for regulating class II HDACs and cardiac hypertrophy. *Cell* **133**, 978–993 (2008).
8. Shao, D. et al. A redox-dependent mechanism for regulation of AMPK activation by thioredoxin1 during energy starvation. *Cell Metab.* **19**, 232–245 (2014).
9. Oka, S. I. et al. Thioredoxin-1 maintains mechanistic target of rapamycin (mTOR) function during oxidative stress in cardiomyocytes. *J. Biol. Chem.* **292**, 18988–19000 (2017).
10. Nagarajan, N. et al. Thioredoxin 1 promotes autophagy through transnitrosylation of Atg7 during myocardial ischemia. *J. Clin. Invest.* **133**, e162326 (2022).
11. Jin, J. K. et al. ATF6 decreases myocardial ischemia/reperfusion damage and links ER stress and oxidative stress signaling pathways in the heart. *Circ. Res.* **120**, 862–875 (2017).
12. Bidwell, P. A. et al. HAX-1 regulates SERCA2a oxidation and degradation. *J. Mol. Cell. Cardiol.* **114**, 220–233 (2018).
13. Ihara, Y., Kageyama, K. & Kondo, T. Overexpression of calreticulin sensitizes SERCA2a to oxidative stress. *Biochem. Biophys. Res. Commun.* **329**, 1343–1349 (2005).
14. Bertero, E. et al. Loss of mitochondrial Ca^{2+} uniporter limits inotropic reserve and provides trigger and substrate for arrhythmias in Barth syndrome cardiomyopathy. *Circulation* **144**, 1694–1713 (2021).
15. Kranias, E. G. & Hajjar, R. J. Modulation of cardiac contractility by the phospholamban/SERCA2a regulatome. *Circ. Res.* **110**, 1646–1660 (2012).
16. Adachi, T. et al. *S*-glutathiolation by peroxynitrite activates SERCA during arterial relaxation by nitric oxide. *Nat. Med.* **10**, 1200–1207 (2004).
17. Goodman, J. B. et al. Redox-resistant SERCA [sarco(endo)plasmic reticulum calcium ATPase] attenuates oxidant-stimulated mitochondrial calcium and apoptosis in cardiac myocytes and pressure overload-induced myocardial failure in mice. *Circulation* **142**, 2459–2469 (2020).
18. Lancel, S. et al. Nitroxyl activates SERCA in cardiac myocytes via glutathiolation of cysteine 674. *Circ. Res.* **104**, 720–723 (2009).
19. Roh, J. D. et al. Activin type II receptor signaling in cardiac aging and heart failure. *Sci. Transl. Med.* **11**, eaau8680 (2019).
20. de Bie, P. & Ciechanover, A. Ubiquitination of E3 ligases: self-regulation of the ubiquitin system via proteolytic and non-proteolytic mechanisms. *Cell Death Differ.* **18**, 1393–1402 (2011).
21. Wei, X. et al. Sigma-1 receptor attenuates osteoclastogenesis by promoting ER-associated degradation of SERCA2. *EMBO Mol. Med.* **14**, e15373 (2022).
22. Doroudgar, S. et al. Hrd1 and ER-associated protein degradation, ERAD, are critical elements of the adaptive ER stress response in cardiac myocytes. *Circ. Res.* **117**, 536–546 (2015).
23. Greenberg, B. et al. Calcium upregulation by percutaneous administration of gene therapy in patients with cardiac disease (CUPID 2): a randomised, multinational, double-blind, placebo-controlled, phase 2b trial. *Lancet* **387**, 1178–1186 (2016).
24. Kho, C. et al. SUMO1-dependent modulation of SERCA2a in heart failure. *Nature* **477**, 601–605 (2011).
25. Stasia, M. J. *CYBA* encoding p22(phox), the cytochrome b558 alpha polypeptide: gene structure, expression, role and physiopathology. *Gene* **586**, 27–35 (2016).
26. Matsushima, S. & Sadoshima, J. Yin and yang of NADPH oxidases in myocardial ischemia–reperfusion. *Antioxidants* **11**, 1069 (2022).
27. Zana, M. et al. Interaction between $p22^{phox}$ and Nox4 in the endoplasmic reticulum suggests a unique mechanism of NADPH oxidase complex formation. *Free Radic. Biol. Med.* **116**, 41–49 (2018).
28. Nakano, Y. et al. Mutation of the *Cyba* gene encoding $p22^{phox}$ causes vestibular and immune defects in mice. *J. Clin. Invest.* **118**, 1176–1185 (2008).
29. Chen, B., Mahaney, J. E., Mayer, M. U., Bigelow, D. J. & Squier, T. C. Concerted but noncooperative activation of nucleotide and actuator domains of the Ca-ATPase upon calcium binding. *Biochemistry* **47**, 12448–12456 (2008).
30. Ravid, T. & Hochstrasser, M. Diversity of degradation signals in the ubiquitin–proteasome system. *Nat. Rev. Mol. Cell Biol.* **9**, 679–690 (2008).
31. Wang, X., Pattison, J. S. & Su, H. Posttranslational modification and quality control. *Circ. Res.* **112**, 367–381 (2013).
32. Meng, F. et al. Oxidation of the cysteine-rich regions of parkin perturbs its E3 ligase activity and contributes to protein aggregation. *Mol. Neurodegener.* **6**, 34 (2011).
33. Zhang, D. D. & Hannink, M. Distinct cysteine residues in Keap1 are required for Keap1-dependent ubiquitination of Nrf2 and for stabilization of Nrf2 by chemopreventive agents and oxidative stress. *Mol. Cell. Biol.* **23**, 8137–8151 (2003).
34. Qi, L., Tsai, B. & Arvan, P. New insights into the physiological role of endoplasmic reticulum-associated degradation. *Trends Cell Biol.* **27**, 430–440 (2017).
35. Cao, S. S. & Kaufman, R. J. Endoplasmic reticulum stress and oxidative stress in cell fate decision and human disease. *Antioxid. Redox Signal.* **21**, 396–413 (2014).
36. Miyano, K. et al. The downregulation of NADPH oxidase Nox4 during hypoxia in hemangioendothelioma cells: a possible role of $p22^{phox}$ on Nox4 protein stability. *Free Radic. Res.* **55**, 996–1004 (2021).
37. Hasenfuss, G. et al. Relation between myocardial function and expression of sarcoplasmic reticulum Ca^{2+}-ATPase in failing and nonfailing human myocardium. *Circ. Res.* **75**, 434–442 (1994).
38. Linck, B. et al. Messenger RNA expression and immunological quantification of phospholamban and SR-Ca^{2+}-ATPase in failing and nonfailing human hearts. *Cardiovasc. Res.* **31**, 625–632 (1996).
39. Meyer, M. et al. Alterations of sarcoplasmic reticulum proteins in failing human dilated cardiomyopathy. *Circulation* **92**, 778–784 (1995).
40. Movsesian, M. A., Karimi, M., Green, K. & Jones, L. R. Ca^{2+}-transporting ATPase, phospholamban, and calsequestrin levels in nonfailing and failing human myocardium. *Circulation* **90**, 653–657 (1994).
41. Munch, G. et al. Unchanged protein expression of sarcoplasmic reticulum Ca^{2+}-ATPase, phospholamban, and calsequestrin in terminally failing human myocardium. *J. Mol. Med.* **76**, 434–441 (1998).

42. Periasamy, M. & Huke, S. SERCA pump level is a critical determinant of Ca^{2+} homeostasis and cardiac contractility. *J. Mol. Cell. Cardiol.* **33**, 1053–1063 (2001).
43. Ragone, I. et al. SERCA2a protein levels are unaltered in human heart failure. *Circulation* **148**, 613–616 (2023).
44. Schwinger, R. H. et al. Unchanged protein levels of SERCA II and phospholamban but reduced Ca^{2+} uptake and Ca^{2+}-ATPase activity of cardiac sarcoplasmic reticulum from dilated cardiomyopathy patients compared with patients with nonfailing hearts. *Circulation* **92**, 3220–3228 (1995).
45. Bers, D. M. Cardiac excitation–contraction coupling. *Nature* **415**, 198–205 (2002).
46. Nickel, A. G. et al. Reversal of mitochondrial transhydrogenase causes oxidative stress in heart failure. *Cell Metab.* **22**, 472–484 (2015).
47. Elzakra, N. et al. Mass spectrometric analysis of SOX11-binding proteins in head and neck cancer cells demonstrates the interaction of SOX11 and HSP90α. *J. Proteome Res.* **16**, 3961–3968 (2017).
48. Saito, T. et al. An alternative mitophagy pathway mediated by Rab9 protects the heart against ischemia. *J. Clin. Invest.* **129**, 802–819 (2019).
49. Del Re, D. P. et al. Yes-associated protein isoform 1 (Yap1) promotes cardiomyocyte survival and growth to protect against myocardial ischemic injury. *J. Biol. Chem.* **288**, 3977–3988 (2013).
50. Calligaris, S. D., Ricca, M. & Conget, P. Cardiac stress test induced by dobutamine and monitored by cardiac catheterization in mice. *J. Vis. Exp.* https://doi.org/10.3791/50050 (2013).
51. Oka, S. et al. PPARα–Sirt1 complex mediates cardiac hypertrophy and failure through suppression of the ERR transcriptional pathway. *Cell Metab.* **14**, 598–611 (2011).
52. Ackers-Johnson, M. et al. A simplified, Langendorff-free method for concomitant isolation of viable cardiac myocytes and nonmyocytes from the adult mouse heart. *Circ. Res.* **119**, 909–920 (2016).
53. Sciarretta, S. et al. Activation of NADPH oxidase 4 in the endoplasmic reticulum promotes cardiomyocyte autophagy and survival during energy stress through the protein kinase RNA-activated-like endoplasmic reticulum kinase/eukaryotic initiation factor 2α/activating transcription factor 4 pathway. *Circ. Res.* **113**, 1253–1264 (2013).
54. Wehrens, X. H. et al. FKBP12.6 deficiency and defective calcium release channel (ryanodine receptor) function linked to exercise-induced sudden cardiac death. *Cell* **113**, 829–840 (2003).
55. Liu, R. et al. Tead1 is required for maintaining adult cardiomyocyte function, and its loss results in lethal dilated cardiomyopathy. *JCI Insight* **2**, e93343 (2017).
56. Zhao, Z. et al. Overexpression of adenylyl cyclase type 5 (AC5) confers a proarrhythmic substrate to the heart. *Am. J. Physiol. Heart Circ. Physiol.* **308**, H240–H249 (2015).

Acknowledgements

We thank D. Zablocki (Rutgers New Jersey Medical School) for critical reading of the paper. This study was supported in part by US Public Health Service grants HL91469, HL112330, HL138720, HL144626 and HL150881 (J.S.). This study was also supported by the American Heart Association Merit Award 20 Merit 35120374 (J.S.) and by the Foundation Leducq Transatlantic Network of Excellence 15CVD04 (J.S.).

Author contributions

Y.N., A.S.T. and J.S. designed the experiments. Y.N., A.S.T., W.M., Y.Y., S.O., T.K. and K.O. conducted the in vitro and in vivo experiments. Y.N., A.S.T. and J.S. wrote the paper. K.T., S.I. and M.M. conducted echocardiographic measurements of the mice. P.Z. conducted the animal experiments and analyses. Y.T. and K.O. conducted immunohistochemistry analyses. N.F., S.H.P. and L.-H.X. performed calcium measurements. T.L. and H.L. performed mass spectrometry and analysis. Y.S. and J.S. generated project resources. All authors reviewed and commented on the paper.

Competing interests

The authors declare no competing interests.

Additional information

Extended data is available for this paper at https://doi.org/10.1038/s44161-025-00699-x.

Supplementary information The online version contains supplementary material available at https://doi.org/10.1038/s44161-025-00699-x.

Correspondence and requests for materials should be addressed to Junichi Sadoshima.

Peer review information *Nature Cardiovascular Research* thanks Christoph Maack, Mark Ranek, Katrin Schroeder and the other, anonymous, reviewer(s) for their contribution to the peer review of this work.

https://doi.org/10.1038/s44161-025-00699-x

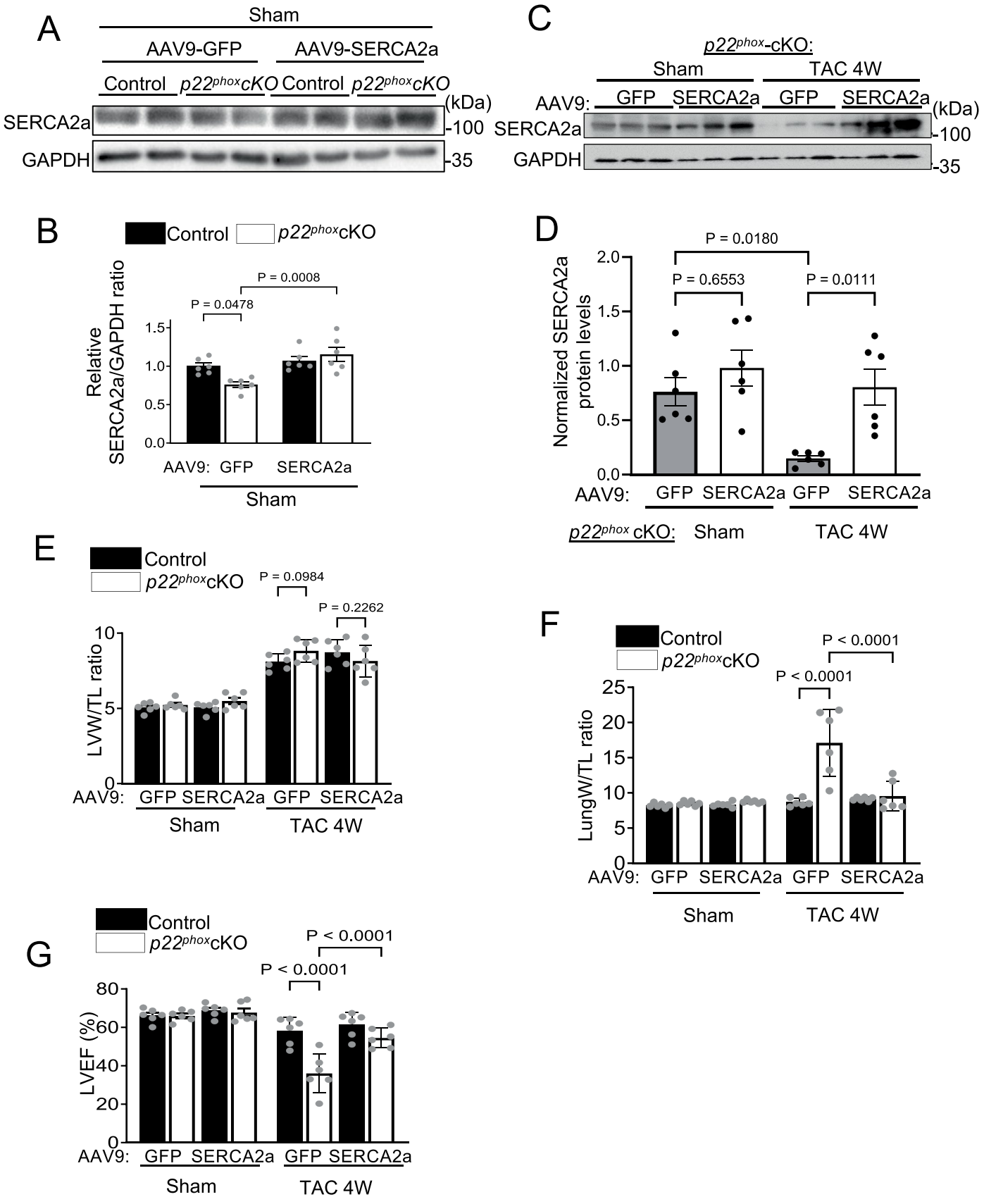

Extended Data Fig. 1 | See next page for caption.

https://doi.org/10.1038/s44161-025-00699-x

Extended Data Fig. 1 | AAV9-mediated SERCA2a overexpression rescues SERCA2a levels and ejection fraction in *p22*^{phox} cKO mice. (**a**–**g**) Control and *p22*^{phox} cKO mice were injected with adeno-associated virus 9 (AAV9) that harbors either GFP or SERCA2a under cTnT promoter one week prior to sham or TAC surgery. Post-surgery the mice were sacrificed at 4-week time point and the following analyses were conducted (**a**) Representative immunoblots showing SERCA2a levels with GAPDH as loading control in control and *p22*^{phox} cKO mice under sham group with adeno-associated virus 9 (AAV9) that harbors either GFP or SERCA2a. (**b**) Relative SERCA2a to GAPDH ratio in (A) (n = 6). (**c**) Representative immunoblots showing SERCA2a levels with GAPDH as loading control in *p22*^{phox} cKO mice under sham and TAC (4 W) condition with adeno-associated virus 9 (AAV9) that harbors either GFP or SERCA2a. (**d**) Quantification of SERCA2a to GAPDH ratio in (C) (n = 6). (**e**) Left ventricle weight to tibia length ratio (LVW/TL ratio) in control and *p22*^{phox} cKO mice under sham and TAC(4 W) condition with adeno-associated virus 9 (AAV9) that harbors either GFP or SERCA2a (n = 6). (**f**) Lung congestion measured as lung weight to tibia length ratio (Lung W/TL ratio) in control and *p22*^{phox} cKO mice under sham and TAC(4 W) condition with adeno-associated virus 9 (AAV9) that harbors either GFP or SERCA2a (n = 6). (**g**) Left ventricle ejection fraction % (LVEF%) measured by echocardiography in control and *p22*^{phox} cKO mice under sham and TAC(4 W) condition with adeno-associated virus 9 (AAV9) that harbors either GFP or SERCA2a (n = 6). All bar graphs are represented as Mean ± SE. The statistical significance was determined with 1-way ANOVA with Tukey test (B, D and F-G) and 1-way ANOVA with Šídák's multiple comparisons test (**e**).

https://doi.org/10.1038/s44161-025-00699-x

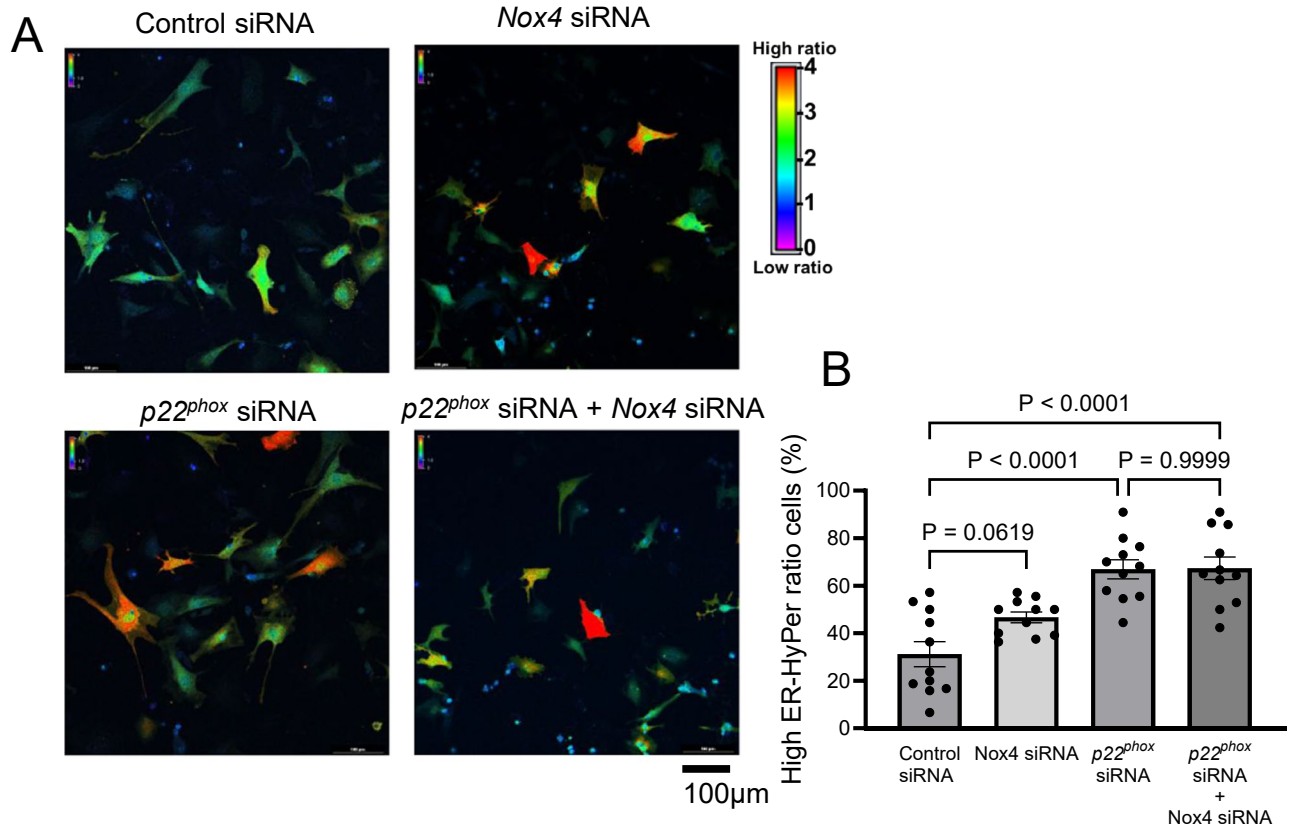

Extended Data Fig. 2 | See next page for caption.

https://doi.org/10.1038/s44161-025-00699-x

Extended Data Fig. 2 | *p22*^{phox} downregulation increases ER-specific H_2O_2 independent of *Nox4*. (**a**, **b**) Neonatal rat cardiomyocytes were transfected with control siRNA, *p22*^{phox} siRNA, *Nox4* siRNA or *p22*^{phox} siRNA + *Nox4* siRNA and transduced with adenovirus harboring ER-localized HyPer. After 48 h incubation, the cells were imaged live under a confocal microscope and the ratiometric image indicating ER H_2O_2 levels was generated and quantified. (**a**) Representative ratiometric image of ER-HyPer fluorescence. Color scale indicates low to high ratio grading. Scale bar = 100 µm. (**b**) Quantification of ER-HyPer high ratio cells in (**a**) ($n = 5$). (**c**–**e**) Neonatal rat cardiomyocytes were transfected with control siRNA, *p22*^{phox} siRNA, *Nox4* siRNA or *p22*^{phox} siRNA + *Nox4* siRNA. *Nox4* was overexpressed as a positive control to identify the specific protein band of *Nox4*. (**c**) Representative immunoblot showing protein levels of SERCA2a, Nox4 and *p22*^{phox} with GAPDH as loading control and Nox OE indicating the specific Nox4 protein band. (**d**, **e**) Quantification of Nox4 and SERCA2a protein levels normalized to GAPDH levels in (**c**) ($n = 9$). All bar graphs are represented as mean + SE. The statistical significance was determined by 1-way ANOVA with Tukey test (**b**, **d** and **e**).

https://doi.org/10.1038/s44161-025-00699-x

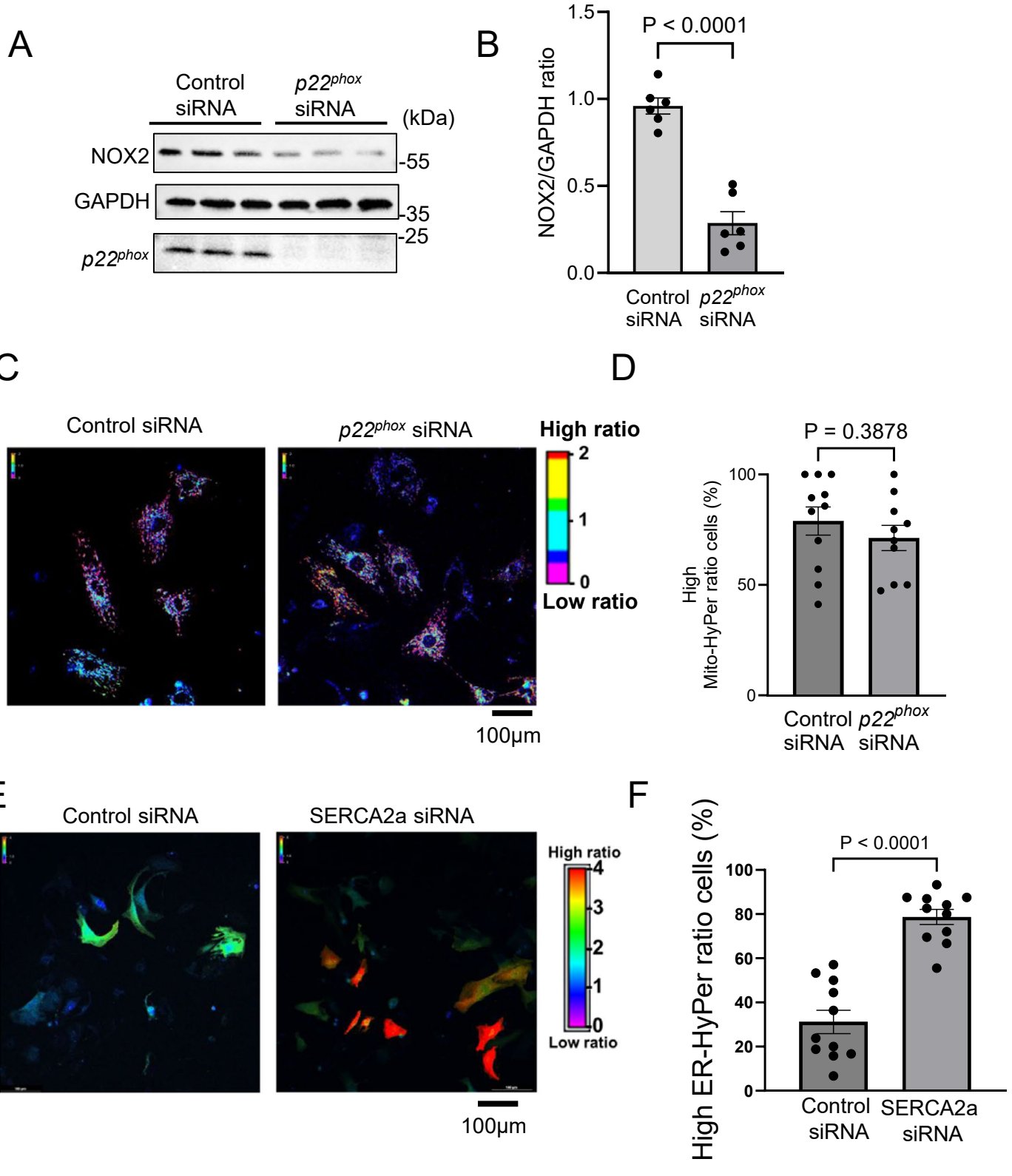

Extended Data Fig. 3 | See next page for caption.

https://doi.org/10.1038/s44161-025-00699-x

Extended Data Fig. 3 | *p22*^{phox} downregulation increases ER-specific H_2O_2 independent of *Nox2* and does not affect mitochondrial H_2O_2 levels. (**a**, **b**) Neonatal rat cardiomyocytes were transfected with the indicated siRNAs and after 48 h the cell lysates were analyzed by Western blotting. (**a**) Representative immunoblot showing protein levels of Nox2 under control siRNA- and *p22*^{phox} siRNA-treated conditions. (**b**) Quantification of Nox2 protein levels expressed as the ratio to GAPDH levels in (**a**) ($n = 6$). (**c**, **d**) Neonatal rat cardiomyocytes were transfected with the indicated siRNAs and transduced with adenovirus harboring mitochondria-localized HyPer. After 48 h incubation, the cells were imaged live under a confocal microscope and the ratiometric image indicating mitochondrial H_2O_2 levels was generated and quantified (**c**). Representative ratiometric image of Mito-HyPer fluorescence. Color scale indicates low to high ratio grading. Scale bar = 100 µm. (**d**) Quantification of Mito-HyPer high ratio cells in (**c**) ($n = 5$). (**e**, **f**) Neonatal rat cardiomyocytes were transfected with the indicated control siRNAs or SERCA2a siRNA and transduced with adenovirus harboring ER-localized HyPer. After 48 h incubation, the cells were imaged live under a confocal microscope and the ratiometric image indicating ER H_2O_2 levels was generated and quantified. (**e**) Representative ratiometric image of ER-HyPer fluorescence. Color scale indicates low to high ratio grading. Scale bar = 100 µm. (**f**) Quantification of ER-HyPer high ratio cells in (**e**) ($n = 5$). All data in bar graphs are represented as mean + SE. The statistical significance was determined with unpaired Student's *t* test (2 tailed) (**b**, **d** and **f**).

https://doi.org/10.1038/s44161-025-00699-x

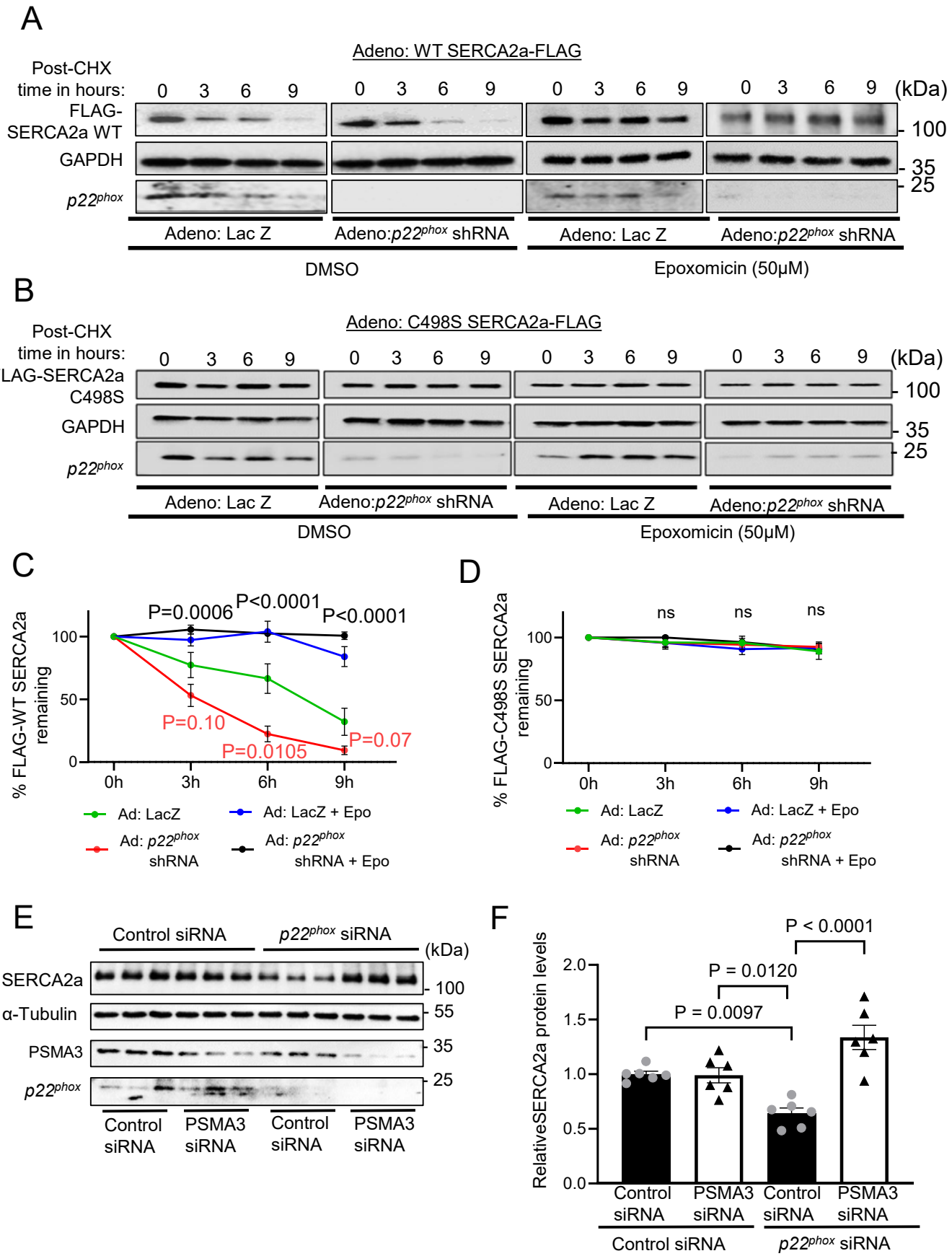

Extended Data Fig. 4 | See next page for caption.

https://doi.org/10.1038/s44161-025-00699-x

Extended Data Fig. 4 | SERCA2a undergoes ubiquitination and proteasomal degradation in the absence of *p22^{phox}*. (**a**–**d**) Neonatal rat ventricular myocytes (NRVM) were transduced with adenovirus harboring either WT SERCA2a-FLAG or SERCA2a (C498S)-FLAG and adenovirus harboring LacZ or *p22^{phox}* shRNA. The stability of SERCA2a was evaluated by pre-incubation (for 1 h) with or without epoxomicin (Epo) (50 μM) (20 s proteasome inhibitor). After treatment with cycloheximide (CHX) (15 μg/ml), cells were collected at 0, 3, 6 and 9 h and analyzed for protein levels of either WT SERCA2a-FLAG or SERCA2a (C498S)-FLAG. (**a**) Representative immunoblots of WT SERCA2a-FLAG post-CHX treatment with or without epoxomicin pre-incubation. (**b**) Representative immunoblots of SERCA2a(C498S)-FLAG post-CHX treatment with or without epoxomicin pre-incubation. (**c**) Quantification of percentage of WT SERCA2a-FLAG plotted for each time point. Each group is indicated by color codes as shown in the graphs. Each dot represents mean ± SE for each time point and connecting lines indicate trend. *P* values indicated in red fonts compare (Ad: Lac Z vs Ad: *p22^{phox}* shRNA groups). *P* values indicated in black fonts compare (Ad: *p22^{phox}* shRNA vs Ad: *p22^{phox}* shRNA + Epo groups) at the respective time points. The *P* values were compared within each timepoint by unpaired Student's *t* test (2 tailed) ($n = 5$). (**d**) Quantification of percentage of SERCA2a (C498S)-FLAG plotted for each time point. Each group is indicated by color codes as shown in the graphs. Each dot represents mean ± SE for each time point and connecting lines indicate trend. The *P* values were compared within each timepoint by unpaired Student's *t* test (2 tailed) and are not significant (ns) ($n = 5$). (**e**, **f**) NRVMs were transfected with control siRNA or *p22^{phox}* siRNA along with PSMA3 siRNA in combinations as indicated in the figure for 48 h, and cell lysates were analyzed by immunoblotting for protein levels of SERCA2a. (**e**) Representative immunoblots of SERCA2a with α-tubulin as loading control from cell lysates after indicated siRNA treatment. (**f**) Quantification of relative SERCA2a levels in (**e**) ($n = 6$). The bar graph is represented as mean ± SE. The statistical significance was determined with 1-way ANOVA with Tukey test.

https://doi.org/10.1038/s44161-025-00699-x

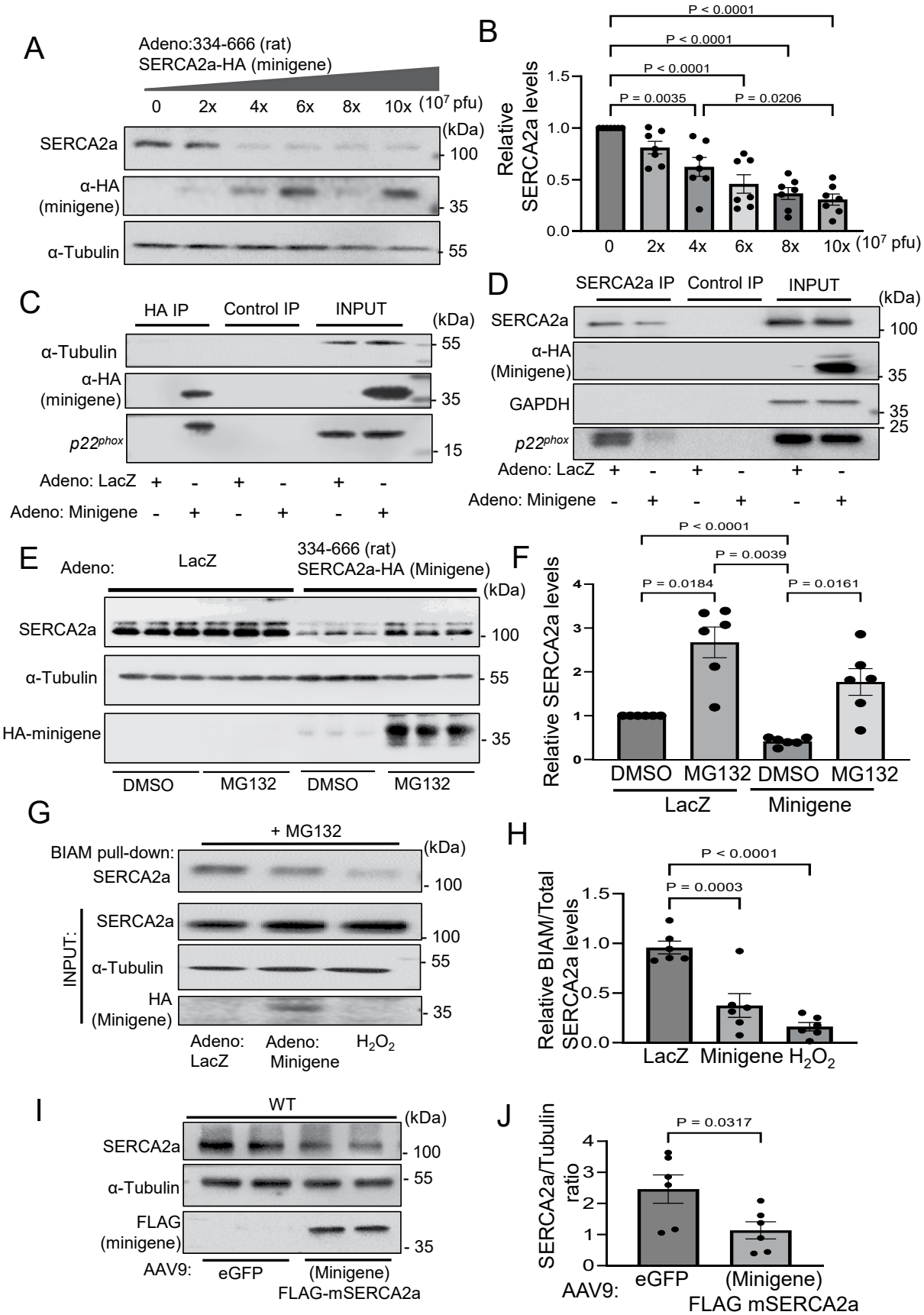

Extended Data Fig. 5 | See next page for caption.

https://doi.org/10.1038/s44161-025-00699-x

Extended Data Fig. 5 | Inhibition of the endogenous interaction between SERCA2a and *p22*^{phox} leads to SERCA2a oxidation and degradation. (**a**) NRVMs were transduced with adenovirus expressing HA-SERCA2a (334-666) fragment (minigene) in increasing amounts as indicated in plaque forming unit (pfu), and cells were collected and analyzed by immunoblotting for SERCA2a protein levels. The figure shows a representative immunoblot of SERCA2a levels with α-tubulin as loading control. The expression of HA-SERCA2a (334-666) fragment is also validated. (**b**) Quantification of SERCA2a levels in (**a**) ($n = 7$). (**c**, **d**) NRVMs were transduced with Ad-HA-SERCA2a (334-666) (minigene) or Ad-LacZ (control) and the cell lysates were immunoprecipitated to study interactions. (**c**) *p22*^{phox} was detected in the anti-HA immunoprecipitate but not in the control immunoprecipitate in Ad-HA-SERCA2a (334-666) (minigene) transduced NRVMs (at least performed three times independently). (**d**) Immunoprecipitation was performed with either anti-SERCA2a or control antibody. The interaction between SERCA2a and *p22*^{phox} was attenuated in the presence of HA-SERCA2a (334-666) (minigene) (at least performed three times independently). (**e**, **f**) NRVMs were transduced with Ad-HA-SERCA2a (334-666) (minigene) or Ad-LacZ (control) and treated with DMSO (vehicle) or MG132 (proteasome inhibitor) and the cell lysates were analyzed for SERCA2a protein levels by immunoblotting. (**e**) Representative SERCA2a immunoblot with GAPDH as loading control shows SERCA2a protein level was stabilized in the presence of MG132 in both the presence and absence of Ad-HA-SERCA2a (334-666) minigene. (**f**) Quantification of relative SERCA2a protein levels in (**e**) ($n = 6$). (**g**) NRVMs were transduced with Ad-HA-SERCA2a (334-666) (minigene) or Ad-LacZ (control) or treated with H_2O_2 (positive control for oxidation) (vehicle). Cells were collected after treatment with MG132 (proteasome inhibitor) for 6 h. Cell lysates were incubated with biotinylated iodoacetamide (BIAM) and pulled down with avidin resin. The pulldown and input fractions were immunoblotted for SERCA2a. SERCA2a oxidation was promoted (indicated by decreases in BIAM pull-down) in the presence of SERCA2a (334-666) and H_2O_2. (**h**) Quantification of BIAM-SERCA2a to total SERCA2a ratio in (**g**) ($n = 6$). (**i**, **j**) AAV9-cTNT-FLAG-mSERCA2a (333-666) or AAV9-cTNT-eGFP was injected into wild type (WT) mice and the level of SERCA2a in the heart was evaluated by immunoblotting. (**i**) Representative immunoblots of SERCA2a with α-tubulin as loading control. FLAG-mSERCA2a (333-666) expression is validated. (**j**) Quantification of SERCA2a to GAPDH ratio in (**i**) ($n = 6$). All bar graphs are represented as mean ± SE. The statistical significance was determined with 1-way ANOVA with Tukey test (**b**, **f**), 1-way ANOVA with Dunnett's multiple comparisons test (**h**) and unpaired Student's *t* test (2 tailed) (**j**).

https://doi.org/10.1038/s44161-025-00699-x

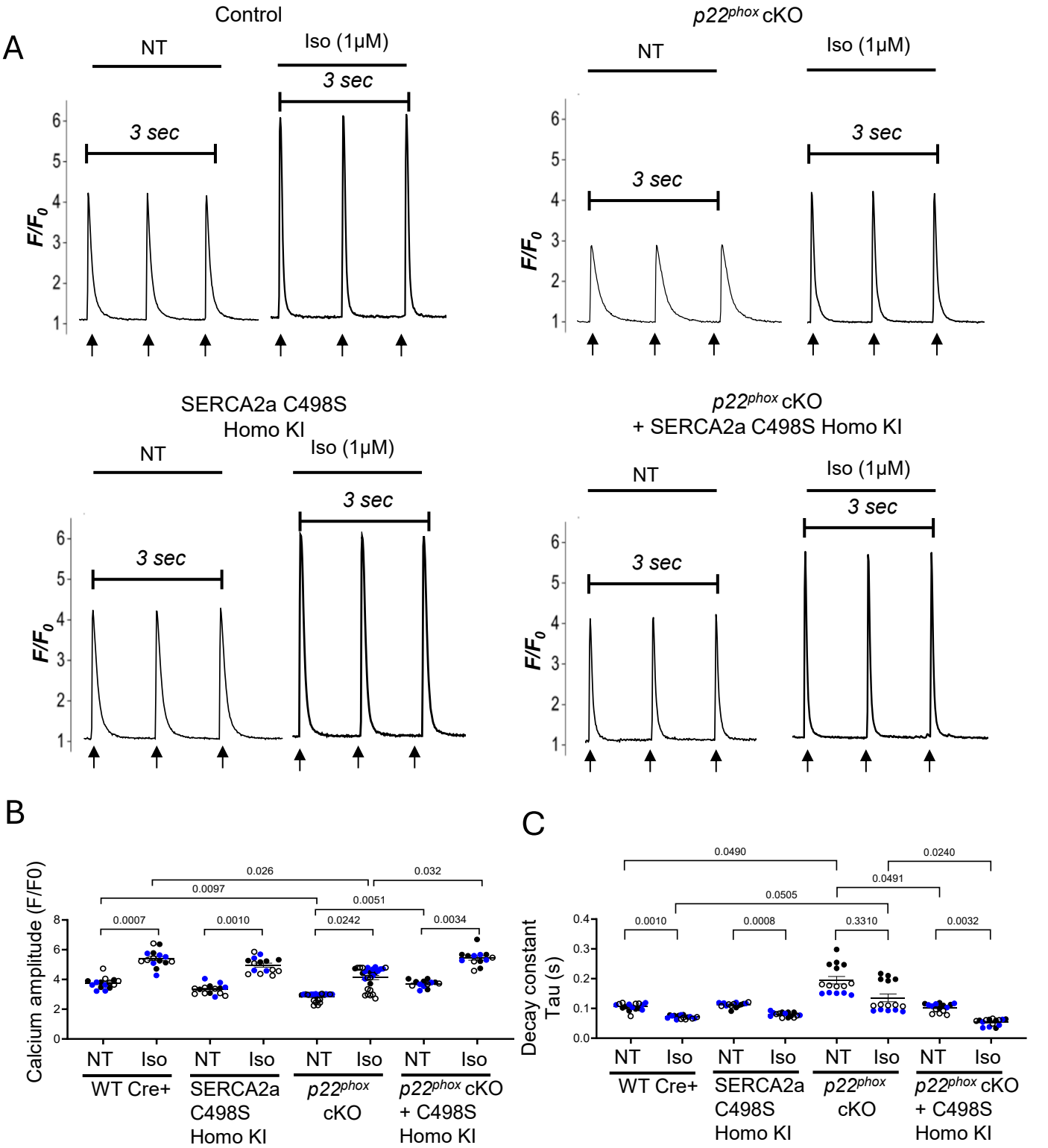

Extended Data Fig. 6 | *SERCA2a C498S* KI restores altered calcium transient in *p22*^{phox} cKO mice. (**a**–**d**) Ca^{2+} transient in WT, *p22*^{phox} cKO. *SERCA2a C498S* homozygous KI and *p22*^{phox} cKO + *SERCA2a C498S* homozygous KI cardiomyocytes at baseline and with isoproterenol (1 μm) stimulation. Adult cardiomyocytes were isolated from respective mice using the Langendorff perfusion method. The cardiomyocytes were loaded with Fluo-4 AM. Ca^{2+} fluorescence intensity was recorded as the ratio of the fluorescence (F) to the basal diastolic fluorescence (F0). (**a**) Representative twitch Ca^{2+} transients under normal Tyrodes (NT) and with isoproterenol (1 μm) (Iso), measured as the height of the peak of Ca^{2+} fluorescence intensity recorded as the ratio F/F0. (**b**, **c**) Summarized data represented as mean ± SE for (**b**) twitch Ca^{2+} transient amplitude (from left to right $n = 5,5,5$; $n = 5,5,5$; $n = 4,4,7$; $n = 4,4,7$; $n = 5,9,10$, $n = 5,9,13$; $n = 6,4,3$; $n = 6,4,3$), (**c**) decay constant (Tau) in (**a**) (from left to right $n = 5,6,5$; $n = 5,6,5$; $n = 5,5,5$; $n = 5,5,5$; $n = 5,5,5$; $n = 5,5,5$; $n = 5,5,5$; $n = 5,5,5$). 3 mice per condition and indicated number of cells per mice were recorded and summarized. The data points from cells of each mouse are represented with distinct color dots (black, blue and black empty). The statistical analysis was conducted using the nested t test (2 tailed) (**b** and **c**) and hierarchical clustering analysis was performed and the dendrogram is provided in the source data file.

https://doi.org/10.1038/s44161-025-00699-x

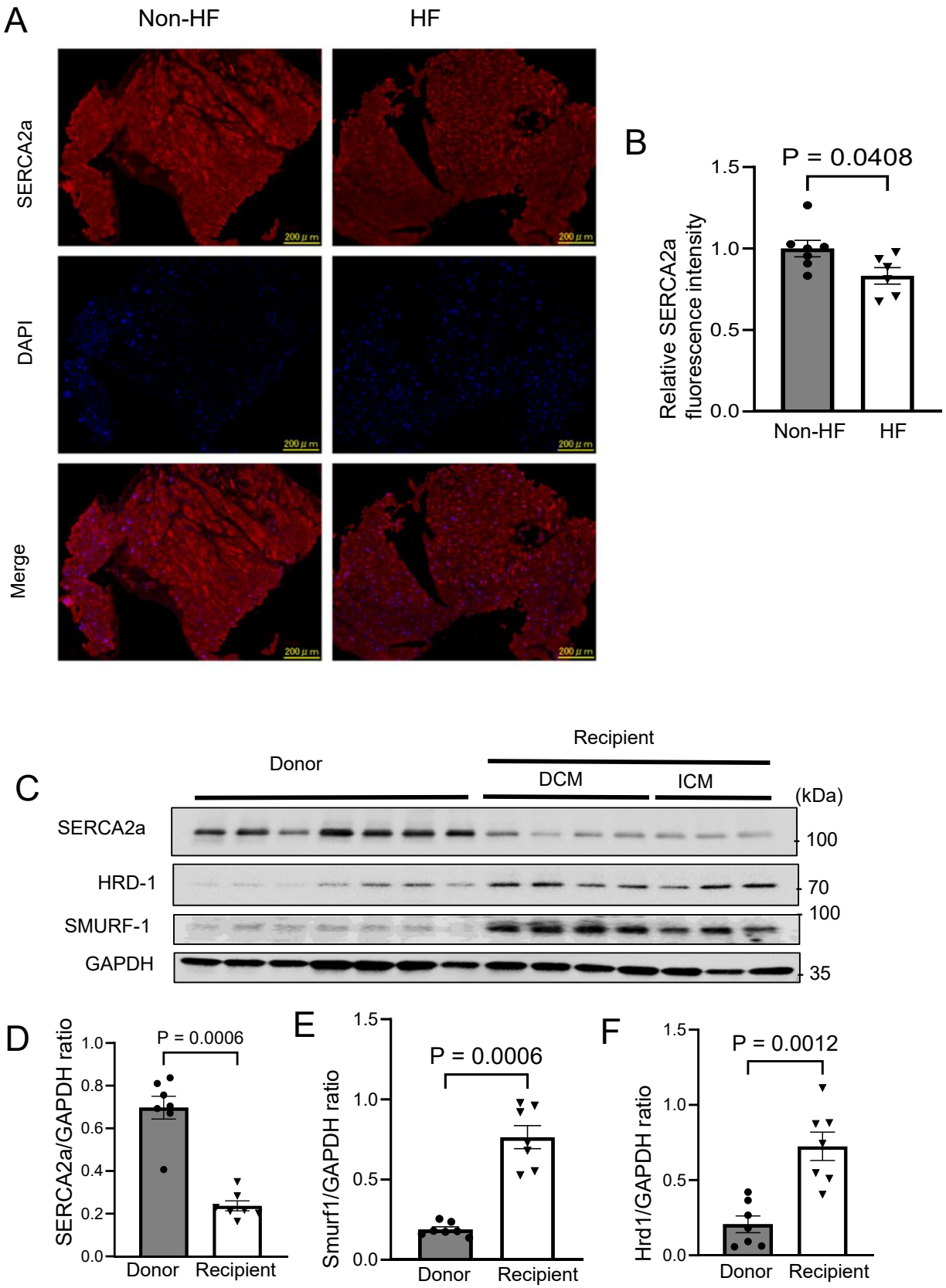

Extended Data Fig. 7 | See next page for caption.

https://doi.org/10.1038/s44161-025-00699-x

Extended Data Fig. 7 | SERCA2a levels negatively correlate with increased Smurf1 and Hrd1 levels in human heart failure samples. (**a**–**f**) Human heart samples obtained from non-heart failure (non-HF) (donors) and heart failure (HF) patients (recipients) were analyzed by immunofluorescence and immunoblotting. (**a**) Representative immunofluorescence staining of non-heart failure (non-HF) (donors) and heart failure (HF) patients with SERCA2a antibody (Red fluorescence) and blue DAPI (nucleus). Scale bar = 200 µm. (**b**) Quantification of the relative SERCA2a fluorescence intensity in non-heart failure (non-HF, $n = 7$) (donors) and heart failure (HF, $n = 6$) patients. (**c**) Immunoblot of lysates from non-heart failure (non-HF) (donors, $n = 7$) and heart failure (HF) patients (recipients, $n = 7$) with dilated cardiomyopathy (DCM, $n = 4$) or ischemic cardiomyopathy (ICM, $n = 3$) showing SERCA2a, Hrd1 and Smurf1 levels, with GAPDH as loading control. (**d**–**f**) Quantification of indicated protein levels as the ratio to GAPDH, compared between donors and recipients. All bar graphs are represented as mean + SE. The statistical significance was determined with unpaired Student's *t* test (2 tailed) (**b**) and the Mann Whitney test (2 tailed) (**d**–**f**).

nature portfolio

Corresponding author(s): Junichi Sadoshima MD, PhD

Last updated by author(s): Jun 25, 2025

Reporting Summary

Nature Portfolio wishes to improve the reproducibility of the work that we publish. This form provides structure for consistency and transparency in reporting. For further information on Nature Portfolio policies, see our Editorial Policies and the Editorial Policy Checklist.

Statistics

For all statistical analyses, confirm that the following items are present in the figure legend, table legend, main text, or Methods section.

n/a	Confirmed	
☐	☒	The exact sample size (*n*) for each experimental group/condition, given as a discrete number and unit of measurement
☐	☒	A statement on whether measurements were taken from distinct samples or whether the same sample was measured repeatedly
☐	☒	The statistical test(s) used AND whether they are one- or two-sided *Only common tests should be described solely by name; describe more complex techniques in the Methods section.*
☒	☐	A description of all covariates tested
☐	☒	A description of any assumptions or corrections, such as tests of normality and adjustment for multiple comparisons
☐	☒	A full description of the statistical parameters including central tendency (e.g. means) or other basic estimates (e.g. regression coefficient) AND variation (e.g. standard deviation) or associated estimates of uncertainty (e.g. confidence intervals)
☐	☒	For null hypothesis testing, the test statistic (e.g. *F*, *t*, *r*) with confidence intervals, effect sizes, degrees of freedom and *P* value noted *Give P values as exact values whenever suitable.*
☒	☐	For Bayesian analysis, information on the choice of priors and Markov chain Monte Carlo settings
☐	☒	For hierarchical and complex designs, identification of the appropriate level for tests and full reporting of outcomes
☒	☐	Estimates of effect sizes (e.g. Cohen's *d*, Pearson's *r*), indicating how they were calculated

Our web collection on statistics for biologists contains articles on many of the points above.

Software and code

Policy information about availability of computer code

Data collection	Data collection method is described in the Method section. Software used: GraphPad Prism 10 Software Image Lab 6.1 ImageJ software (NIH) (https://imagej.nih.gov/ij/download.html) Imaris 10.0.1.
Data analysis	Data collection method is described in the Method section. Software used: GraphPad Prism 10 Software Image Lab 6.1 ImageJ software (NIH) (https://imagej.nih.gov/ij/download.html) Imaris 10.0.1.

For manuscripts utilizing custom algorithms or software that are central to the research but not yet described in published literature, software must be made available to editors and reviewers. We strongly encourage code deposition in a community repository (e.g. GitHub). See the Nature Portfolio guidelines for submitting code & software for further information.

Data

Policy information about availability of data

All manuscripts must include a data availability statement. This statement should provide the following information, where applicable:

- Accession codes, unique identifiers, or web links for publicly available datasets
- A description of any restrictions on data availability
- For clinical datasets or third party data, please ensure that the statement adheres to our policy

All original data underlying selected data shown in the figures and supplemental figures are available from the corresponding author upon reasonable request.

Research involving human participants, their data, or biological material

Policy information about studies with human participants or human data. See also policy information about sex, gender (identity/presentation), and sexual orientation and race, ethnicity and racism.

Reporting on sex and gender	The human heart samples were from males and female between the age 26-77. The detailed information on the samples are provide in Supplementary Table S1,S2 and S3.
Reporting on race, ethnicity, or other socially relevant groupings	The sample are obtained from donors and patients at Taipei Veterans General Hospital (Taiwan) and Nara Medical University (Japan).
Population characteristics	The sex, age and cardiac disease classification of the human subjects shown in this study are summarized in Supplemental Table S1,S2 and S3. Age range is 26-77, both male and female.
Recruitment	The samples were recruited at random based on availability in residual sample bank and no conflict of interest.
Ethics oversight	The samples from explanted hearts used in this study (Figure 1A and Figure 11C) were obtained from donors and patients who had undergone heart transplantation at Taipei Veterans General Hospital, Taiwan (Supplemental Table S1). The study was approved by the Ethics Committee of Taipei Veterans General Hospital, and all specimens from residual sample bank, Taipei Veterans General Hospital. The IRB number is Taipei VGH IRB no. 2018-05-006BC. The human tissue immunofluorescence data in Figure 11A was performed at Nara Medical University, Japan (Supplemental Table S1). The study protocols were approved by the Nara Medical University Ethics Committee, G107, and has followed the 1975 Declaration of Helsinki guidelines. Written informed consent to collect tissue, conduct research and to publish results anonymously was obtained from all participants and/or their legal guardians prior to collection

Note that full information on the approval of the study protocol must also be provided in the manuscript.

Field-specific reporting

Please select the one below that is the best fit for your research. If you are not sure, read the appropriate sections before making your selection.

☒ Life sciences ☐ Behavioural & social sciences ☐ Ecological, evolutionary & environmental sciences

For a reference copy of the document with all sections, see nature.com/documents/nr-reporting-summary-flat.pdf

Life sciences study design

All studies must disclose on these points even when the disclosure is negative.

Sample size	The sample size employed in this study was determined based on the minimum number required to attain statistical significance. The estimated sample size was n = 5-8 per group, as derived from a power analysis informed by our preceding studies that investigated the effects of pressure overload, prolonged ischemia, and ischemia/reperfusion injury on the heart. These studies include, but are not limited to, reference 9 (Nagarajan, N et al. J Clin Invest 2022), reference 44 (Saito, T. et al. J Clin Invest 2019) and reference 45 (Del Re, D.P. et al. J Biol Chem 2013) of this paper.
Data exclusions	Mice that did not survive the procedures of transverse aortic constriction surgery were excluded.
Replication	In vivo experimental findings were reproducible as shown across multiple animals over multiple surgical cohorts. In vitro experimental findings were independently reproduced at least 3 times unless specified. All attempts at replication were successful.
Randomization	Mice were not randomized because they were genetically identical within groups. The relevant experimental controls were used in each experiment as described in this paper.
Blinding	Transverse aortic constriction surgeries, echocardiography and histopathology data collection and analysis, were conducted by investigators who were blinded to the genetic backgrounds of the mice and the experimental treatments. However, certain Western blot data were acquired by investigators aware of the genetic backgrounds and experimental treatments to determine the sequence in which samples should be loaded onto the gels.

Reporting for specific materials, systems and methods

We require information from authors about some types of materials, experimental systems and methods used in many studies. Here, indicate whether each material, system or method listed is relevant to your study. If you are not sure if a list item applies to your research, read the appropriate section before selecting a response.

Materials & experimental systems

n/a	Involved in the study
☐	☒ Antibodies
☒	☐ Eukaryotic cell lines
☒	☐ Palaeontology and archaeology
☐	☒ Animals and other organisms
☒	☐ Clinical data
☒	☐ Dual use research of concern
☒	☐ Plants

Methods

n/a	Involved in the study
☒	☐ ChIP-seq
☒	☐ Flow cytometry
☒	☐ MRI-based neuroimaging

Antibodies

Antibodies used

1) ATP2A2/SERCA2 Rabbit Ab, Cell Signaling Technology, #4388S, Lot:2 (WB- 1:1000).
2) Goat pAb to SERCA2 ATPase, abcam, #AB219173, Lot: 1002614-2 (IF- 1:200).
3) CYBA polyclonal Ab (p22phox), Invitrogen, #PA5-75653, Lot: ZC4256465 (WB- 1:1000, IP).
4) Rb mAb to SERCA2 ATPase (EPR9392), abcam, #Ab150435, Lot:1006533-14 (IP)
5) PSMA3 (D4Y90) Rabbit mAb, Cell Signaling Technology, #12446S, Lot:1 (WB-1:1000).
6) PSMA3 Rabbit Poly Ab, pproteiroteintech, #11887-1-AP, Lot:00058001 (IF-1:200).
7) Monoclonal Anti-SMURF-1, Clone 1D7 antibody produced in mouse, SIGMA-ALDRICH, #WH0057154M1-100UG, Lot:K1201-1D7 (WB-1:1000).
8) GAPDH (14C10) Rabbit mAb, Cell Signaling Technology, #2118S, Lot:16 (WB-1:5000).
9) DYKDDDDK Tag (D6W5B) (FLAG-tag), Cell Signaling Technology, #14793S, Lot:7 (WB-1:1000).
10) HA-tag (C29F4) Rabbit mAb, Cell Signaling Technology, #3724S, Lot:10 (WB-1:1000, IP).
11) Anti-α-Tubulin antibody, Mouse monoclonal clone DM1A, purified from hybridoma cell culture, Merck-Millipore, #T6199-200UL, Batch: 0000180310 (WB-1:1000).
12) HRD1/SYVN1 mouse Mc Ab, proteintech, #67488-1-Ig, Lot:10014875 (WB-1:1000, IF-1:100).
13) Rb mAb to Ubiquitin (EP8589) (linkage-specific k48), abcam, #Ab140601, Lot:1006904-15 (WB-1:1000).
14) Dityrosine monoclonal antibody (10A6), Invitrogen, #MA5-27566, Lot:VJ3104731`(WB-1:1000).
15) Phospholamban (D9W8M) Rabbit mAb, Cell Signaling Technology, #14562, (WB-1:1000)
16) Phospho-Phospholamban (Ser16/Thr17) Antibody, Cell Signaling Technology, #8496, (WB-1:1000)
17) Mouse anti Rabbit light chain-HRP (clone-SBS62a), Bio-Rad, #MCA6003P, Lot:180730 (WB-1:5000).
18) Mouse anti-Rabbit IgG conformation-specific (L27A9) mAb (HRP), Cell Signaling Technology, #5127S, Lot:11 (WB-1:5000).
19) Anti-rabbit IgG HRP-linked antibody, Cell Signaling Technology, #7074S, Lot:26 (WB-1:5000).
20) Anti-mouse IgG HRP-linked antibody, Cell Signaling Technology, #7076S, Lot:38 (WB-1:5000).
21) Anti-NOX4 Rabbit PolyAb, proteintech, #14347-1-AP, Lot:00100525 (WB-1:1000)
22)Anti-NOX2/gp91phox Rb mAb (EPR6991), abcam, #129068, Lot:GR3229874

Validation

All antibodies utilized in this study are commercially available. The manufacturers have validated the specificity of all commercially available antibodies through knockout/knockdown experiments, confirmed their reactivity in the intended species, and assessed their compatibility with the respective applications. Additionally, the specificity of the antibodies was confirmed by in the knockdown experiments shown by this study especially Smurf1, Hrd1 and PSMA3. The ATP2A2/SERCA2 (#4388S) antibody was validated by knockdown using specific siRNA and over-expression in rat noenatal cardiomyocytes in this study and the blots are available for verification on request.

Animals and other research organisms

Policy information about studies involving animals; ARRIVE guidelines recommended for reporting animal research, and Sex and Gender in Research

Laboratory animals

All mice included in this study were on a C57Bl/6J genetic background. Mouse strains used in this study include p22phox flox/flox Mh6 Cre+ mice and ATP2A2(SERCA2a) C498S knock-in mice which were generated in house (detailed in methods) and backcrossed with C57Bl/6J wild-type mice which were purchased from Jackson Labs. All mice used in this study ranged from 2 to 4 months of age depending on the experiments. One-day-old Crl:(WI) BR-Wistar rats (Envigo, Somerville) were used for isolation of primary cultures of neonatal ventricular cardiomyocytes.

Wild animals

No wild animals were used in this study.

Reporting on sex

In general, the estrogen and its cycle in female mice impact on studying hypertrophy and heart failure. In addition, the mortality and

Reporting on sex	morbidity of cardiovascular diseases are sex-dependent. Therefore, only male mice were used in our animal studies.
Field-collected samples	No field-collected samples were used in this study.
Ethics oversight	All experimental procedures involving mice received approval from the Institutional Animal Care and Use Committee at Rutgers New Jersey Medical School (Protocol numbers: IACUC PROTOCOL 201900187) in accordance with the Guide for the Care and Use of Laboratory Animals published by the U.S. National Institutes of Health.

Note that full information on the approval of the study protocol must also be provided in the manuscript.

Plants

Seed stocks	N/A
Novel plant genotypes	N/A
Authentication	N/A